Agenzia Nazionale per le Nuove Tecnologie,
l'Energia e lo Sviluppo Economico Sostenibile

Ministero dello Sviluppo Economico

RICERCA DI SISTEMA ELETTRICO

CERSE-POLIMI RL 1137/2010

HDRB isolating devices: criteria for FE modeling and failure characterization

G. Bianchi, Corradi dell'Acqua, M. Domaneschi, D. Mantegazza, F. Perotti

Report RdS/2010/90

HDRB ISOLATING DEVICES: CRITERIA FOR FE MODELLING AND FAILURE CHARACTERIZATION

G. Bianchi, Corradi dell'Acqua, M. Domaneschi, D. Mantegazza, F. Perotti

Settembre 2010

Report Ricerca di Sistema Elettrico
Accordo di Programma Ministero dello Sviluppo Economico – ENEA
Area: Produzione e fonti energetiche
Tema: Nuovo Nucleare da Fissione

Responsabile Tema: Stefano Monti, ENEA

CIRTEN

CONSORZIO INTERUNIVERSITARIO

PER LA RICERCA TECNOLOGICA NUCLEARE

POLITECNICO DI MILANO

DIPARTIMENTO DI INGEGNERIA STRUTTURALE

DIPARTIMENTO DI ENERGIA

HDRB isolating devices: criteria for FE modeling and failure characterization

AUTORI

L. Corradi dell'Acqua
F. Perotti
G. Bianchi
D. Mantegazza
M. Domaneschi

CIRTEN-POLIMI RL 1137

Milano, September 2010

Lavoro svolto in esecuzione della linea progettuale LP2 punto I3 - AdP ENEA MSE del 21/06/07
Tema 5.2.5.8 – "Nuovo Nucleare da Fissione".

Introduction and scope

The present report describes the research activity performed at Politecnico di Milano within the field of seismic isolation of NPP buildings, with particular reference to the IRIS case. In this activity the development of reliable and efficient FE HDRB models in ANSYS® has been pursued along with the and definition of a reasonable limit state failure domain under seismic excitation.

In a first phase of the activity a complete FE HDRB model was set, detailed in the first sections (1, 2) of this report. Subsequently, extensive numerical tests were performed to identify the most suitable material model among those provided by the software.

In the second phase it was deemed to be more effective to focus further analyses only on the rubber layer, rather than on the full isolator. This approach gives a desirable tighter control over constitutive law phenomenology, allows to neglect interaction between rubber ad steel and helps to reduce model size, accelerating the route to a robust material definition to be implemented in the final isolator model.

Thus, the content of subsequent sections of the present report refers to a single layer of rubber, whose material properties and geometry are detailed in § 3 and in § 4.

Specific scopes of the document are:

1. identify limit state conditions. Since new regulations (EN 15129) prescribe to estimate both "complete failure" (rupture) and "first damage" conditions under low and high occurrence probability seismic events, respectively (as summarized in § 0), and considering that rupture experiments results are not yet available, first damage condition is investigated here. Moreover, it can be confidently based on equivalent stress peaks derived from an hyperelastic FE model;
2. evaluate reliability and validity domain of the analytical approach developed by (Corradi et al. 2009) that proposes a closed formula for stresses in a rubber layer, subjected separately to vertical and horizontal loading, based on an hyperelastic (9 parameters Mooney-Rivlin constitutive law) problem solution, formulated in large displacement. The validity of this theory could significantly reduce the computational cost of "first damage" limit state domain statement;
3. quantify the problem nonlinearity at high horizontal strain values (300%) by evaluating the error in stress values between a reference FE solution, where rubber layer is subjected to horizontal and vertical force simultaneously, and the superposition of two FE solutions where the same forces are applied separately. As stated for scope 2, this approach could lead to computational savings in domain definition;
4. insert current work into new European Norm frame (EN 15129).

These scopes are mainly functional to accomplish step 2 and step 4 of the procedure described by (De Grandis et al. 2009), which proposes an innovative approach for the evaluation of seismic isolator system fragility. In particular, they can be summarized as follows:

- step 1: performance of experimental tests;
- step 2: development a refined FE model of the isolator, taking into account all significant sources of mechanical and geometrical nonlinearities; the model, after having been validated with experimental results, will be used to simulate additional and more complex numerical tests;
- step 3: calibration based on experimental tests;
- step 4: statement of the limit state condition for the isolator, expressing the interaction between horizontal and vertical load at failure;
- step 5: isolation system fragility analysis.

1. Phase 1: material model requirements and ANSYS capabilities

In order to reproduce accurately NPP (Nuclear Power Plant) seismic response, the material model shall exhibit the following features:

- nonlinear stiffness;
- displacement dependent (hysteretic) damping;

while other features, like:

- small progressive increase of hysteretic cycles amplitude;
- temperature dependence;

are judged to be numerically negligible, considering the scope of analyses. Shear stiffness dependence on vertical and biaxial horizontal load will be investigated.

Other modelling strategies, such as lumped linear viscoelastic or bilinear models, are not investigated, since they could exhibit good performance just at a prescribed strain level. Moreover, as reported in (Grant et al. 2005), where an equivalent viscous damping is calculated for a certain peak displacement excursion, cycles at lower levels of displacement will typically be overdamped. Moreover, viscous damping has been recognized as negligible compared to hysteretic (Forni 2009).

The so called “Mullins’s effect”, or “scragging”, is still being investigated in order to evaluate if it is relevant in design phase and/or safety analysis, but is believed to be negligible so far. It is mainly related to stiffness degradation that makes possible to distinguish between virgin and preconditioned specimens and suggests bidirectional coupling (deformation in one direction degrades stiffness in the orthogonal direction as well), but in literature (Thompson et al. 2000, Clark et al. 1997) the phenomenon is believed to be recoverable and maybe due to the compound.

In order to reproduce the hysteretic damping behaviour, various authors proposed different models in the last thirty years. As reported in (Forni et al. 2009), the damping force may be considered as a hysteretic, rate-independent effect (Kikuchi and Aiken 1997), or as a viscoelastic dissipation that depends on the strain rate (Hwang, 2002). Tsai [2003] recently proposed a model based on a Bouc-Wen (Bouc 1967) approach, coupled with a linear viscious term. All these models require the identification of a large number of material parameters. The large strain constitutive response of filled elastomers has been extensively studied, including hyperelastic, viscoelastic and viscoplastic models. Recent models my (Miehe and Keck 2000) and (Haupt and Sedlan 2001) consider all three of these aspects of elastomer behaviour, represented rheologically by a number of appropriately defined springs in parallel.

(Abe et al. 2004) extended an elastoplastic model by adding a displacement-dependent isotropic hardening rule and the parallel nonlinear elastic spring

Several phenomenological models are summarized in (Grant et al. 2005):

- Unidirectional models: classical linear and bilinear models (Hwang 2002, Kikuchi and Aiken 1997, Tsai et al. 2003):
- Plasticity-based models (accounting for bidirectional behavior): classical plasticity with kinematic hardening, bounding surface model, bounding and stiffening surfaces model (Grant et al. 2005).

Among reported materials models, ANSYS® isotropic hyperelastic models are listed, commonly adopted to reproduce a static loading path (command: TBDATA with TB, HYPER):

- Neo-hookean, with 2 parameters;
- Mooney-Rivlin, with 2, 3, 5 or 9 parameters;
- Polynomial form, with N^2+N parameters;
- Ogden, with 3N parameters (3N-2 independent);
- Arruda-Boyce, with 3 parameters;
- Gent, with 3 parameters;
- Yeoh, with 2N parameters;
- Ogden compressive foam, with 2N parameters;
- Blatz-Ko, with 1 parameter;
- User-defined subroutine;

All output stresses are computed from the second Piola-Kirchoff stresses.

Since the superposition of hydrostatic pressure in incompressible materials makes the following stress states equivalent:

- uniaxial tension and equibiaxial compression;
- uniaxial compression and equibiaxial tension;
- planar tension (plain strain) and planar compression;

three independent stress states should be performed to define material parameter.

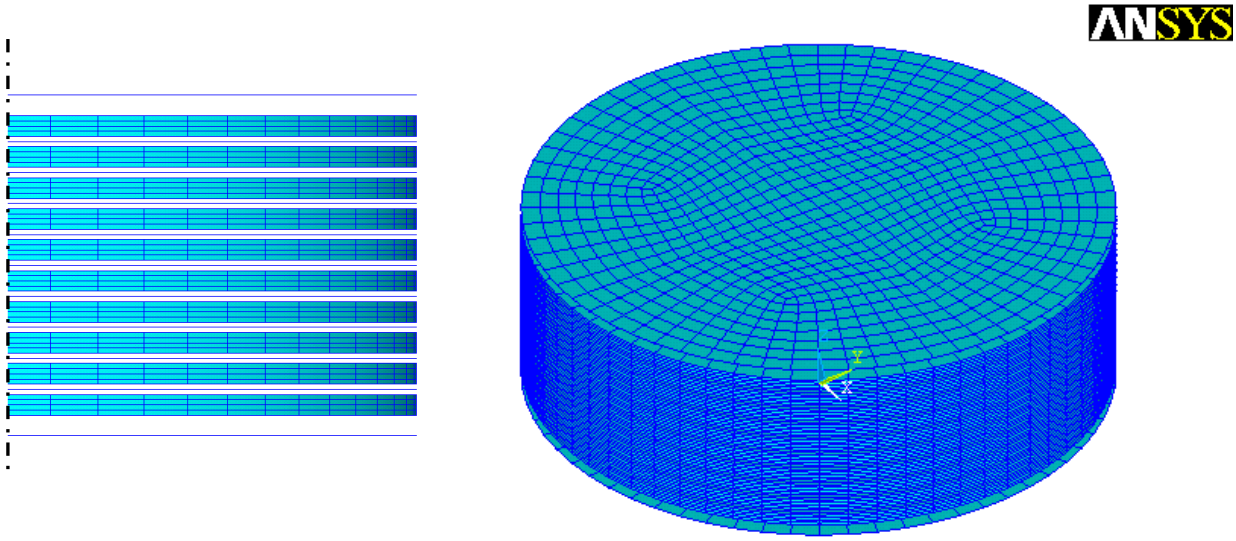

2. Phase 1: criteria for FE modelling

After having considered and studied experimental results, phenomenological aspects, constitutive HDRB laws and having examined ANSYS® capabilities, the following modelling strategy has been chosen to start HDRB 3D analysis:

- *parametric geometry and mesh generation*: solid discs simulating high-damping rubber (three elements layers) + interposed shell elements for middle steel plates; model generation has been implemented via parametric macro;
- *constraint*: shell nodes have translational DOF tied to aligned solid elements nodes by means of rigid links.
- *finite elements*: SOLID186 for solid elements (higher order 3D 20-node element with quadratic displacement behaviour, suitable to model curved boundaries; it supports plasticity, hyperelasticity, creep, stress stiffening, large deflection, large strain; its formulation can simulate nearly incompressible elastoplastic and fully incompressible hyperelastic materials); SHELL281 for shell steel elements (4+4 node elements with 3+3 DOF at each node, allowing for finite membrane strains);
- *material*: TBD

3. Phase 2: rubber properties for FE analysis

In order to evaluate the static and dynamic behaviour of HDRB and their ultimate capacity for vertical and horizontal loading, a series of tests were performed at ISMES - CESI laboratories (Bergamo, June 2010) and at FIP Industries laboratories (Padova, June 2010) on scaled isolators specimens. Since experimental data are not completely available at the moment, analyses results reported here are based on hard rubber properties derived from the same source **Errore. L'origine riferimento non è stata trovata.** that was adopted by Corradi et al. in [1] for analytical rubber model tuning.

Reference rubber parameters are as follows:

- E = 2.40 MPa
- G = 0.80 MPa
- ν = 0.50

The experimental curve underwent a least square fitting procedure in order to estimate Mooney - Rivlin hyperelastic constitutive law parameters, resulting in:

- c_{10} = 0.08455 MPa
- c_{20} = 0.03170 MPa
- c_{30} = -6.710E-4 MPa

with reference to the following classical Mooney – Rivlin elastic potential energy formula:

$$W = c_{10}(I_1 - 3) + c_{01}(I_2 - 3) + c_{20}(I_1 - 3)^2 + c_{11}(I_1 - 3)(I_2 - 3) + c_{02}(I_2 - 3)^2 + c_{30}(I_1 - 3)^3 + + c_{21}(I_1 - 3)^2(I_2 - 3) + c_{12}(I_1 - 3)(I_2 - 3)^2 + c_{03}(I_2 - 3)^3$$

where all other six non-zero parameters were forced at zero, following the approach in [3].

4. Phase 2: ANSYS® FE model and analysis parameters

To investigate the behaviour of a single HD rubber layer, the following modelling strategy has been chosen, considering literature experimental results, phenomenological aspects, HD rubber constitutive laws and ANSYS® capabilities:

- *parametric geometry and mesh generation*: the high-damping rubber single layer model generation has been implemented via parametric macro with variable geometry and mesh density. At the top and at the bottom face, a rigid steel plate has been modeled as a node with a rigid link with the rubber disc upper and lower face.

	VARIABLE PARAMETER	ADOPTED
GEOMETRY	Diameter (D)	250 mm
	Rubber layer th. (sr)	2.5 mm
MESH	N. of element in each rubber layer th. (e)	6
	Typical dimensions of brick elements (es)	3.33, 3.33, 0.42 [mm] (x, y, z)
	N. of DOF (half isolator)	70000

- *constraints*: the connection between the upper and lower nodes and the rubber surfaces is provided by means of rigid links. Just half isolator has been modeled and symmetry constraint were set at DOF laying on XZ plane;
- *finite elements*: SOLID185 element for bricks (linear 3D 8-node element with 3 DOF at each node, with plasticity, hyperelasticity, stress stiffening, creep, large deflection, and large strain capabilities. It also has mixed formulation capability for simulating deformations of nearly incompressible elastoplastic materials, and fully incompressible hyperelastic materials). The chosen integration method is the Uniform Reduced Integration with hourglass control (ANSYS Theoretical Manual);
- *material*: (see § 3);
- *boundary conditions and loads*: top and bottom nodes are used to impose all loads and boundary conditions to the model. Vertical and horizontal actions are always applied by means of vertical force in Z direction and horizontal displacement in X direction, respectively. Bottom node is always fixed (Ux = Uy = Uz = Rx = Ry = Rz = 0), while upper node BCs depend on the analysis case and scope (see § 1), as follows

Analysis cases are listed in the following table, as referenced in results figures (§ 4.1, § 4.2 and § 4.3):

ANALYSIS CASE	RESTRAINED DOF AT UPPER NODE	APPLIED LOAD F_z [N]	APPLIED DISP. U_x [mm]
1.a	U_x, U_y, R_x, R_y, R_z	80000	0
1.b	U_y, R_x, R_y, R_z	-	7.5
2.a	U_y, U_z, R_x, R_y, R_z	-	7.5
3.a	U_y, R_x, R_y, R_z	80000	7.5

Target final displacement applied in this highly geometric and mechanical nonlinear analysis (horizontal displacement to rubber layer height ratio is up to 300%) needed special cautions and required extensive work to choose the most suitable finite element formulation, mesh definition, step increment and nonlinear analysis parameters to obtain convergence, which was found to be highly affected by vertical to horizontal loads ratio.

4.1 Results – scope 1 (stress analysis)

Stress analysis results are reported here in the form of contour lines draw on isolator vertical and horizontal sections and stress graph along loading paths, with reference to analysis ID listed in § 4:

Vertical loading (analysis case 1.a):

- Sigma_z (horizontal section 1 @100% Vmax)
- Sigma_z (vertical section 2 @100% Vmax)
- Sigma_t (horizontal section @100% Vmax)
- Sigma_t (vertical section 2 @100% Vmax)
- Sigma_r (horizontal section 11@100% Vmax)
- Sigma_r (vertical section 2 @100% Vmax)
- Tau_zr (horizontal section 1 @100% Vmax)
- Tau_zr (vertical section 2 @100% Vmax)
- sigma Von Mises (horizontal section 1 @100% Vmax)
- sigma Von Mises (vertical section 2 @100% Vmax)

Horizontal loading (analysis case 1.b):

- sigma_x (2x horizontal section 1 @150%,300% Hmax)
- sigma_x (2x vertical section 2 @150%,300% Hmax)
- tau_zx (2x horizontal section 1 @150%,300% Hmax)
- tau_zx (2x vertical section 2 @150%,300% Hmax)
- sigma Von Mises (2x horizontal section 1 @150%,300% Hmax)
- sigma Von Mises (2x vertical section 2 @150%,300% Hmax)

- 3 x 2 stress graphs, along loading path (sigma x at TA and MA points, tau_xz at TA and MA points, sigma Von Mises at TB and MB points).

- Fx and My reaction force and moment at top node.

4.2 Results – scope 2 (validation of (Corradi et al. 2009) model)

Stress analysis results are reported here in the form of stress graph, with reference to analysis ID listed in § 4:

Vertical loading (analysis case 1.a and analytical solution):

- 2 x 2 stress graphs (FE and analytical), along radial path (sigma_z along path M, tau_zr along path T).

Horizontal loading (analysis case 2.a and analytical solution):

- 3 x 2 stress graphs, along loading path (FE and analytical, sigma x at MA point, sigma_z at MA point, tau_zr at MA point).

- Fx, Fz and My reaction forces and moment at top node.

4.3 Results – scope 3 (superposition)

Stress analysis results are reported here in the form of stress graph, with reference to analysis ID listed in §4:

Horizontal and vertical loading (analysis cases 3.a, 1.a+1.b):

- 3 figures containing 2 + 2 + 2 stress graph gathered at 300% horizontal displacement and Vmax, along radial path T (combination and superposition for sigma_z, tau_xz, sigma Von Mises)

- 3 figures containing 2 + 2 + 2 stress graph gathered at 300% horizontal displacement and Vmax, along radial path M (combination and

superposition for sigma_z, tau_xz, sigma Von Mises)

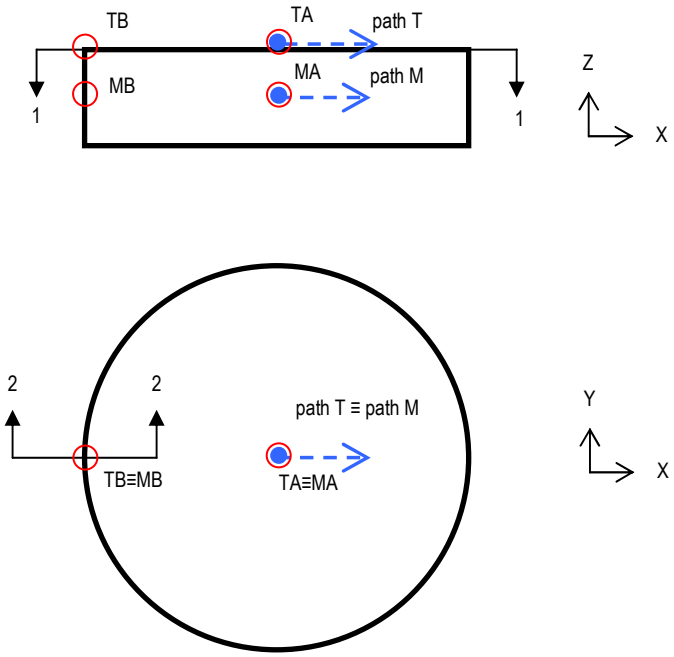

5. European Norm 15129:2009

In order to insert current analyses into a modern regulation frame, some general prescription for anti-seismic devices, contained in chapter 4 "General design rules" of (UNI EN 15129), are summarized here:

- 4.1.1 "Fundamental requirements": some "non failure" and "damage limitation", for severe and serviceability seismic events respectively, are stated. "Damage limitation" has to be intended as the definition of a damage that does not require replacement,
- 4.1.4 "Structural and mechanical requirements": The device and its connections to the structure should be designed so that, for a seismic action beyond the design seismic action (ultimate limit state), there is no immediate catastrophic failure or immediate change in the properties sufficient to be detrimental to the dynamic behaviour of the structure. They shall retain a residual capacity at least equal to the permanent actions to which they are directly subjected or to such combinations of actions corresponding to design situations (including eventually a seismic situation) that may occur after the earthquake.
Furthermore, isolation devices shall be designed with higher reliability then the whole structure, by introducing a magnification factor on design actions (1.20 or 1.50, as recommended in EUROCODE 8, EN1998-1 for elastomeric isolators in and in EN1998-2 respectively). It has to be noted that §4.3.1 clarifies that this increment is functional to reduce seismic analysis uncertainties.

6. Future activities

Further analyses are being developed in order to accomplish final objectives described in §1 for the evaluation of isolator system fragility. In particular, future work will include:

- analysis of experimental results (see § 3) to tune Mooney – Rivlin parameters;
- analysis of experimental results (see § 3) to investigate first damage and ultimate capacity of the isolator, for horizontal and vertical loads separately;
- proceed in HDRB FE full model development with Mooney Rivlin hyperelastic constitutive law;
- limit state domain definitions, based on comparison between FE analyses and experimental failure modes.

References

[1] Abe M., Yoshida J., Fujino Y. (2004), "Multiaxial Behaviors of Laminated Rubber Bearings and Their Modeling. II: Modeling", *ASCE Journal of Structural Engineering*, 130:8, 1133-1144.
[2] ANSYS Release 12, Theoretical manual.
[3] Bouc R. (1967), "Forced vibration of mechanical system with hysteresys", *Proceedings of Fourth Conference on Nonlinear Oscillation*, Prague, Czechoslovakia.

[4] Cai C., Zheng H., Khan M.S., Hung K.C., "Modeling of Material Damping Properties in ANSYS", *CADFEM Users' Meeting & ANSYS Conference*, October 9-11 2002, Friedrichshafen, Germany.

[5] Clark P., Aiken I.D., Kelly J.M. (1997), "Experimental studies of the ultimate behaviour of seismically-isolated structures", *Technical Report UCB/EERC-97/18*, Earthquake Engineering Research Center.

[6] Corradi dell'Acqua L., Domaneschi M., Guiducci C., "Assessing the reliability of seismic base isolators for innovative power plant proposals", *20th International Conference on STRUCTURAL MECHANICS IN REACTOR TECHNOLOGY (SMIRT20)*, August 9-14, 2009, Espoo Finland.

[7] De Grandis S., Domaneschi M., Perotti F., "A numerical procedure for computing the fragility of NPP components under random seismic excitation", *Nuclear Engineering and Design*, Volume 239, Issue 11, November 2009, Pages 2491-2499, ISSN 0029-5493, DOI: 10.1016/j.nucengdes.2009.06.027.

[8] UNI EN 15129:2009 – Anti-seismic devices.

[9] EN 1998 Eurocode 8 - Design of structures for earthquake resistance.

[10] Forni M., Martelli A., Dusi A., Castellano G., "Hyperelastic Models of Steel – Laminated Rubber Bearings for Seismic Isolation of Civil Buildings and Industrial Plants", *Proceedings of the International ABAQUS User's Conference*, May 31- June 2 1995, Paris, France, 273-287.

[11] Forni M.– Private communication 24/07/09.

[12] Forni M., Poggianti A., Bianchi F., Forasassi G., Lo Frano R., Pugliese G., Perotti F., Corradi dell'Acqua L., Domaneschi M., D. Carelli M., Ahmed A.M., Maioli A., "Seismic Isolation of the IRIS Nuclear Plant", *Proceedings of the 2009 ASME pressure Vessel and Piping Conference*, *PVP 2009*, July 26-30, 2009, Prague, Czech Republic.

[13] Grant D.N., Fenves G.L., Auricchio F. (2005), "Modelling and analysys of high-damping rubber bearings for the seismic protection of bridges", *Research Report No. ROSE-2005/01*, ROSE School, Collegio Alessandro Volta, Via Ferrata, 27100, Pavia, Italy.

[14] Haupt P. and Sedlan K. (2001), "Viscoplasticity of elastomeric materials: experimental facts and constitutive modelling", *Archive of Applied Mechanics*, 71:89-109.

[15] Huang W.-H. (2002), Bi-directional testing, modeling, and system response of seismically isolated bridges", Ph.D. Thesis, University of California, Berkeley.

[16] Kikuchi M. and Aiken I.D. (1997), "An analytical hysteresis model for elastomeric seismic isolation bearings", *Earthquake Engineering and Structural Dynamics*, 26:215-231.

[17] Miehe C. and Keck J.(200), Superimposed finite elastic-viscoelastic-plastoelastic stress response with damage in filled rubbery polymers. Experiments, modelling, and algorithmic implementation", *Journal of the Mechanics of Phisics and Solids*, 48:323-365.

[18] Thompson A.C.T., Whittaker A.S., Fenves G.L., Mahin S.A. (2000), "Property modification factors for elastomeric seismic isolation bearings", *Proceedings of the 12th World Conference on Earthquake Engineering*, Auckland, New Zealand.

[19] Tsai C.S., Chiang T.-C., Chen B.-J. And Lin S.-B. (2003), "An advanced analytical model for high damping rubber bearings", *Earthquake Engineering and Structural Dynamics*, 32:1373-1387.

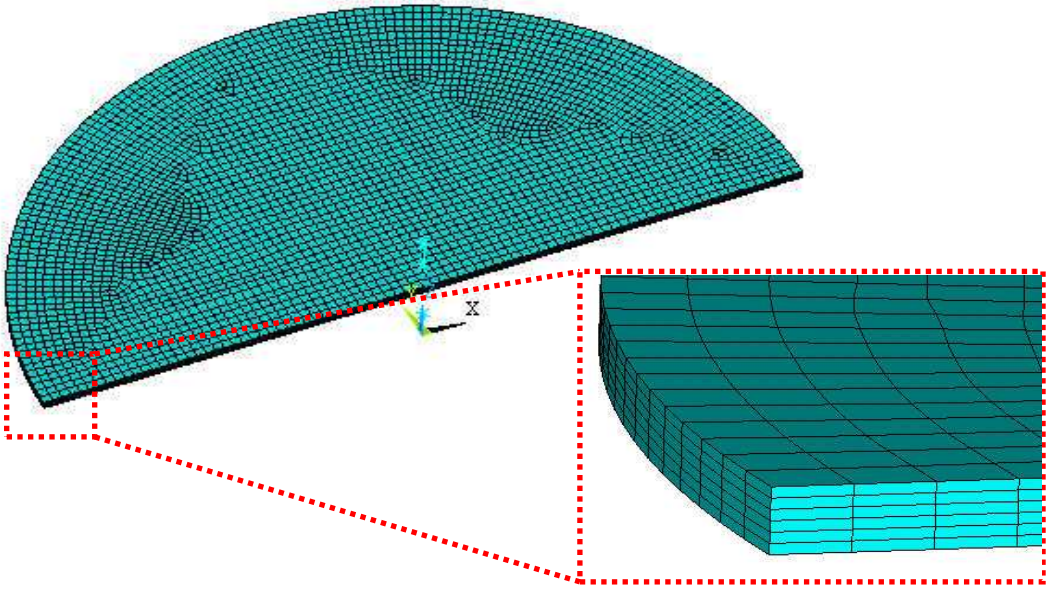

4.1 - sigma z (h. sections @100% Vmax)

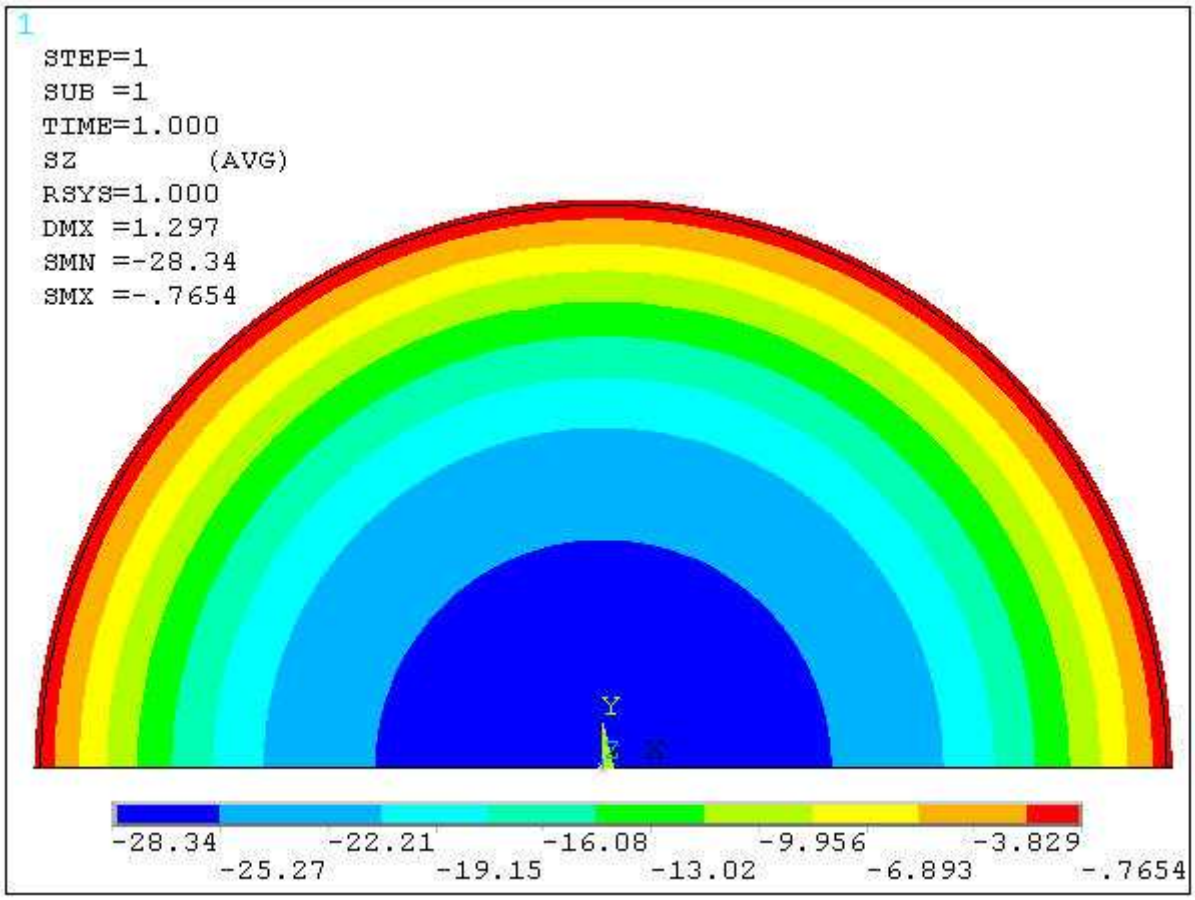

4.1 - sigma z (v. sections @100% Vmax)

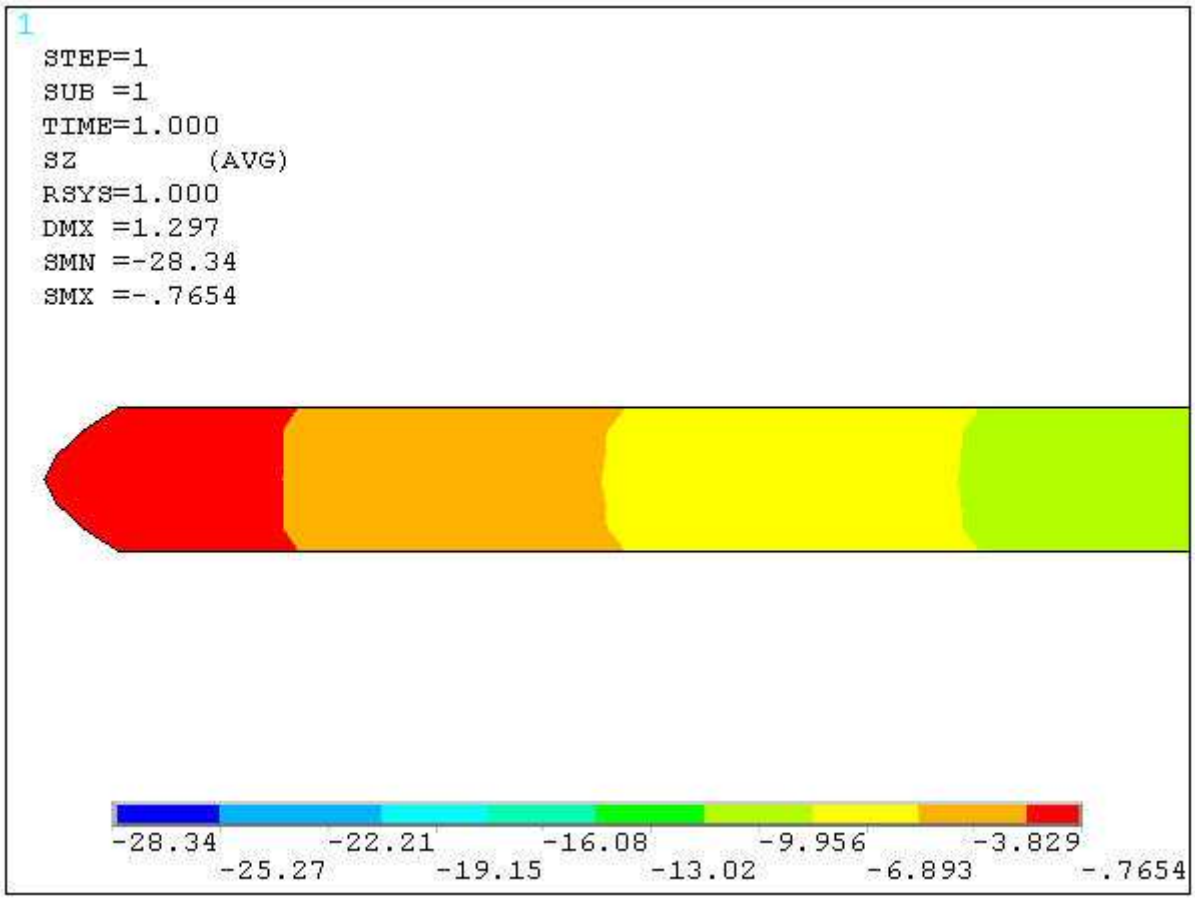

4.1 - sigma t (h. sections @100% Vmax)

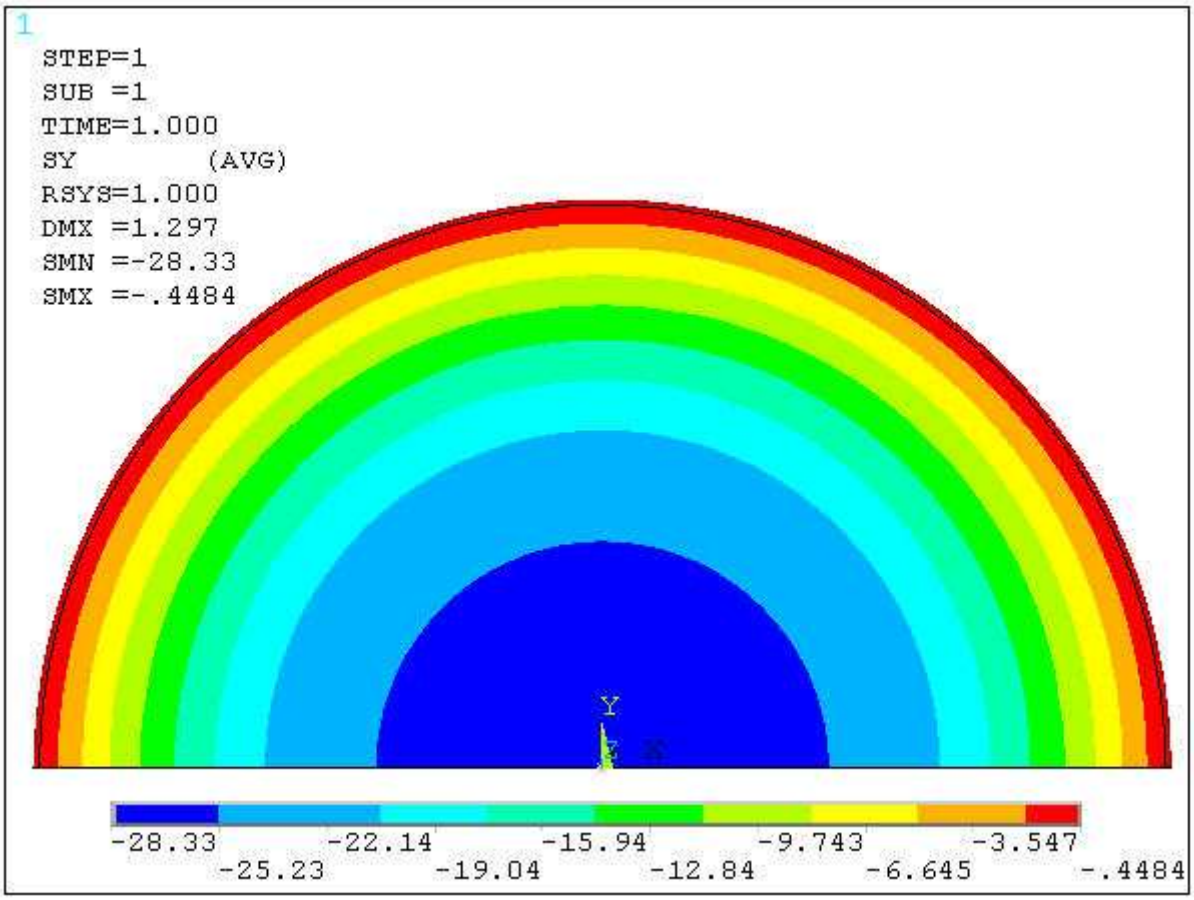

4.1 - sigma t (v. sections @100% Vmax)

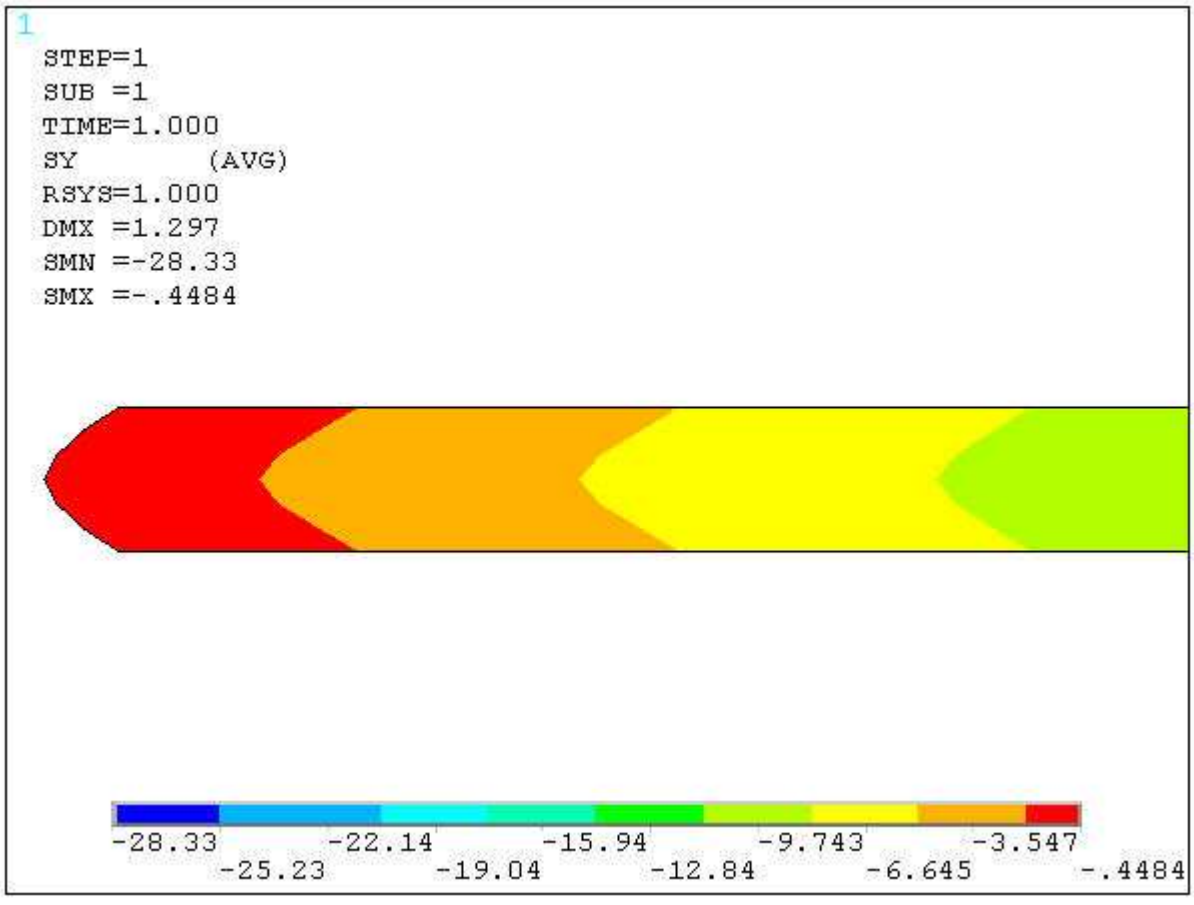

4.1 - sigma r (h. sections @100% Vmax)

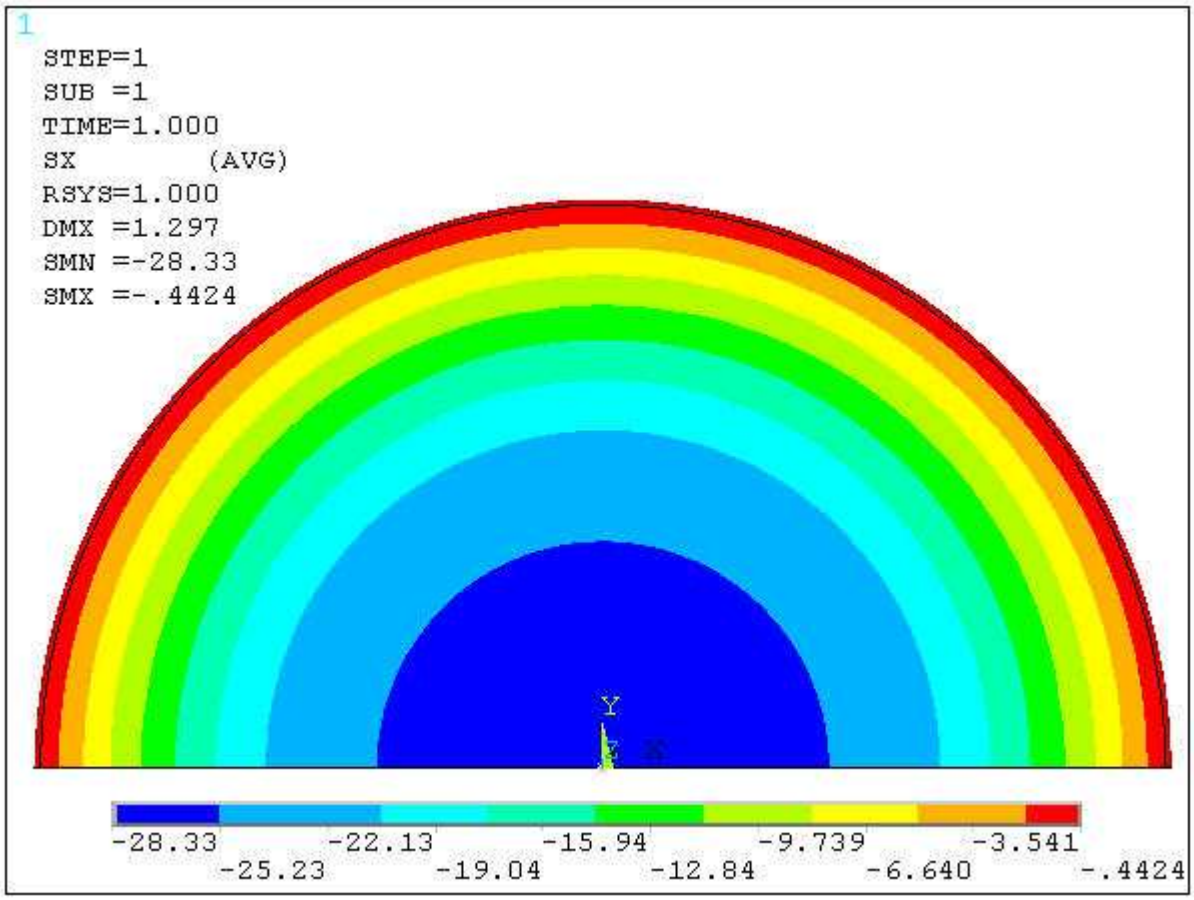

4.1 - sigma r (v. sections @100% Vmax)

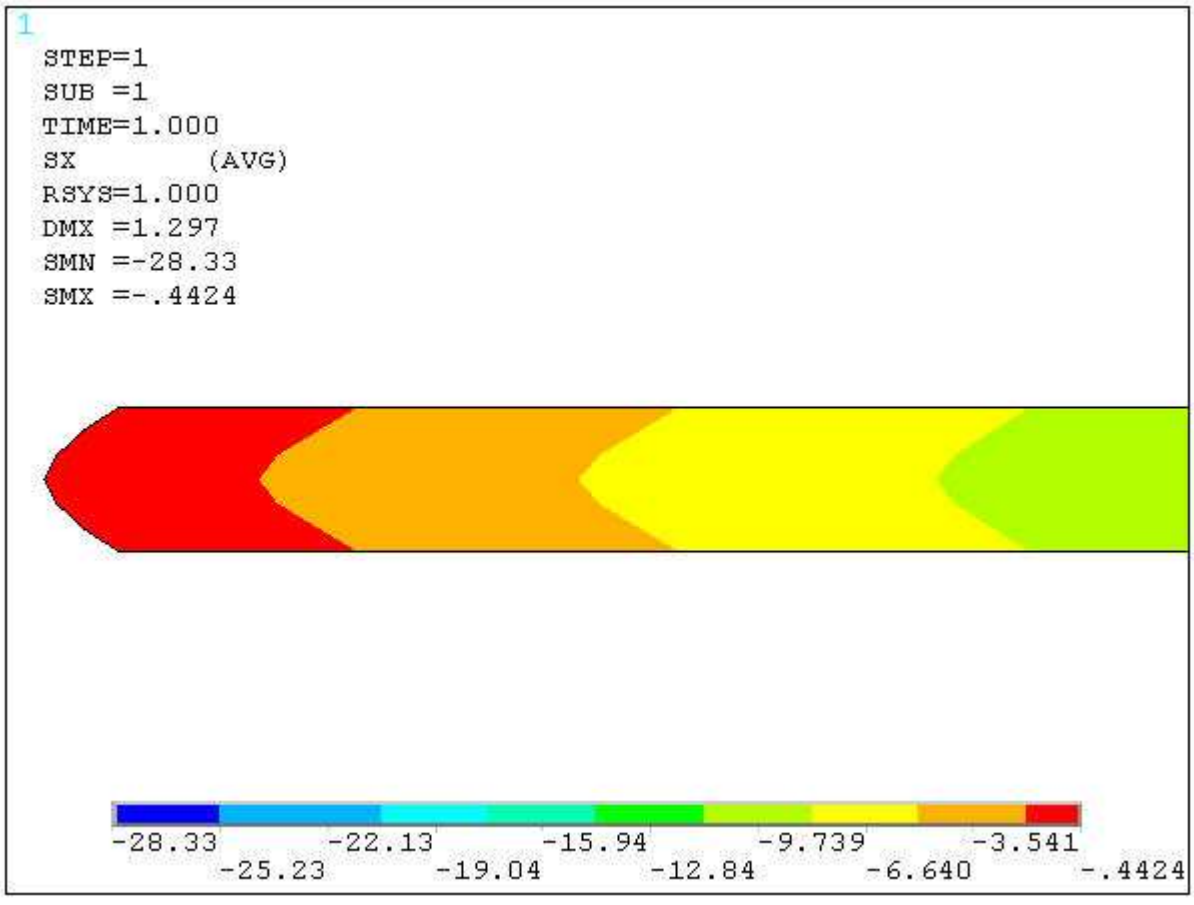

4.1 - tau zr (h. sections @100% Vmax)

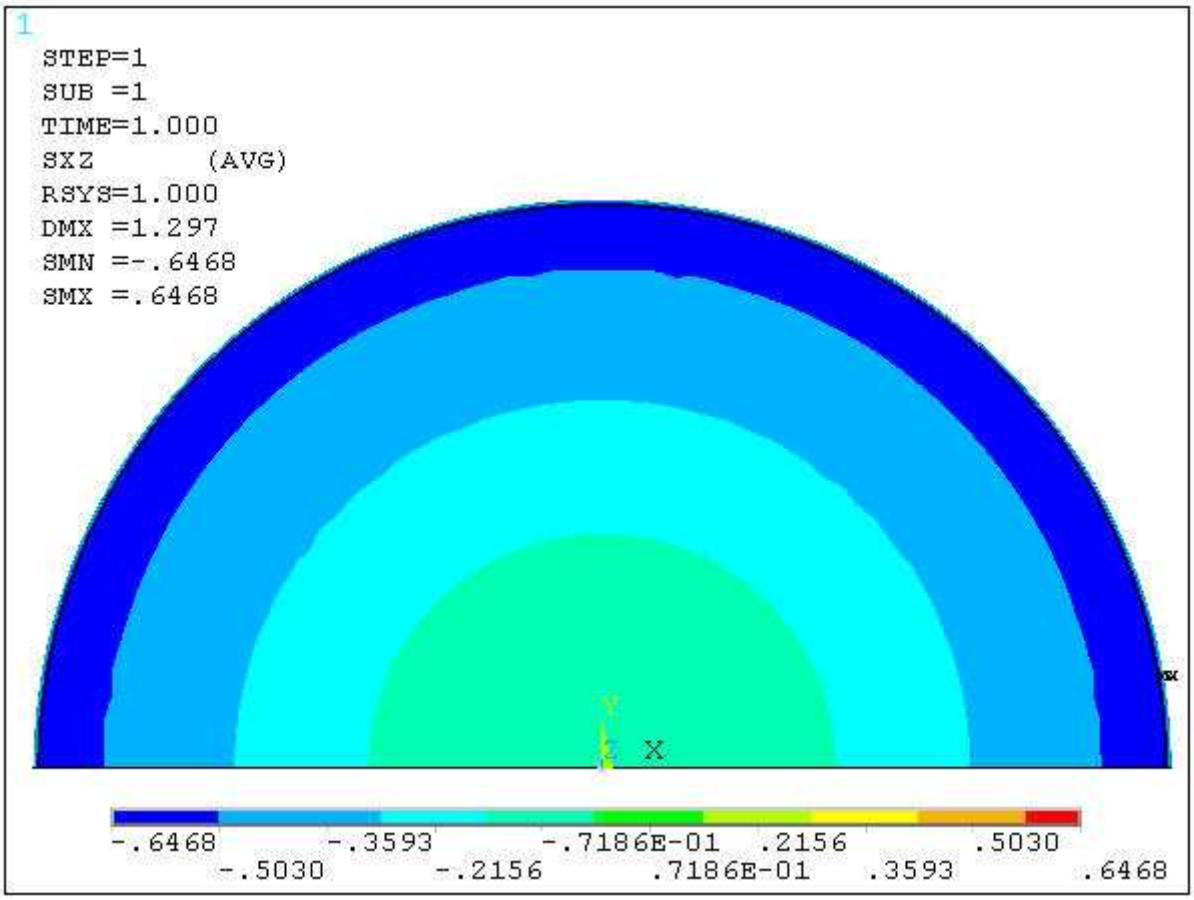

4.1 - tau zr (v. sections @100% Vmax)

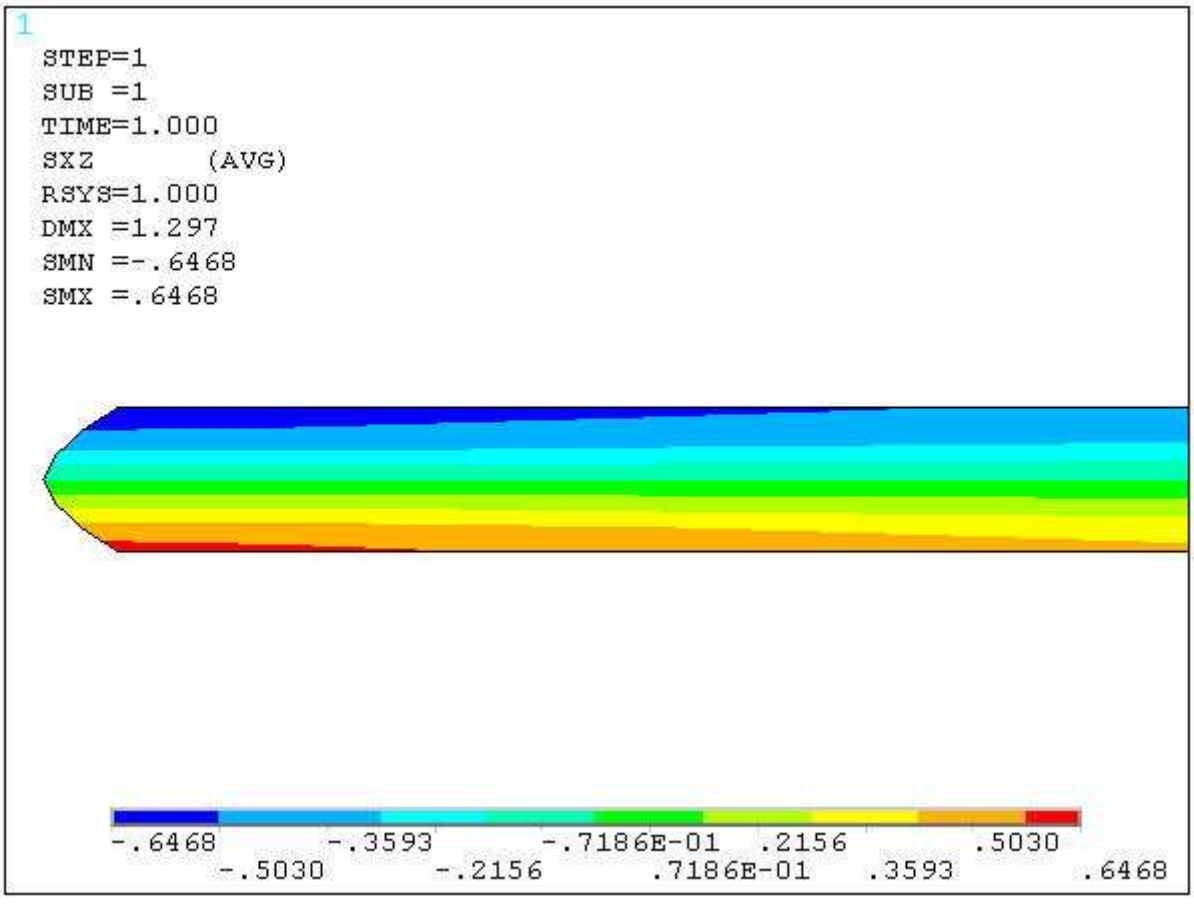

4.1 - sigma Von Mises (h. sections @100% Vmax)

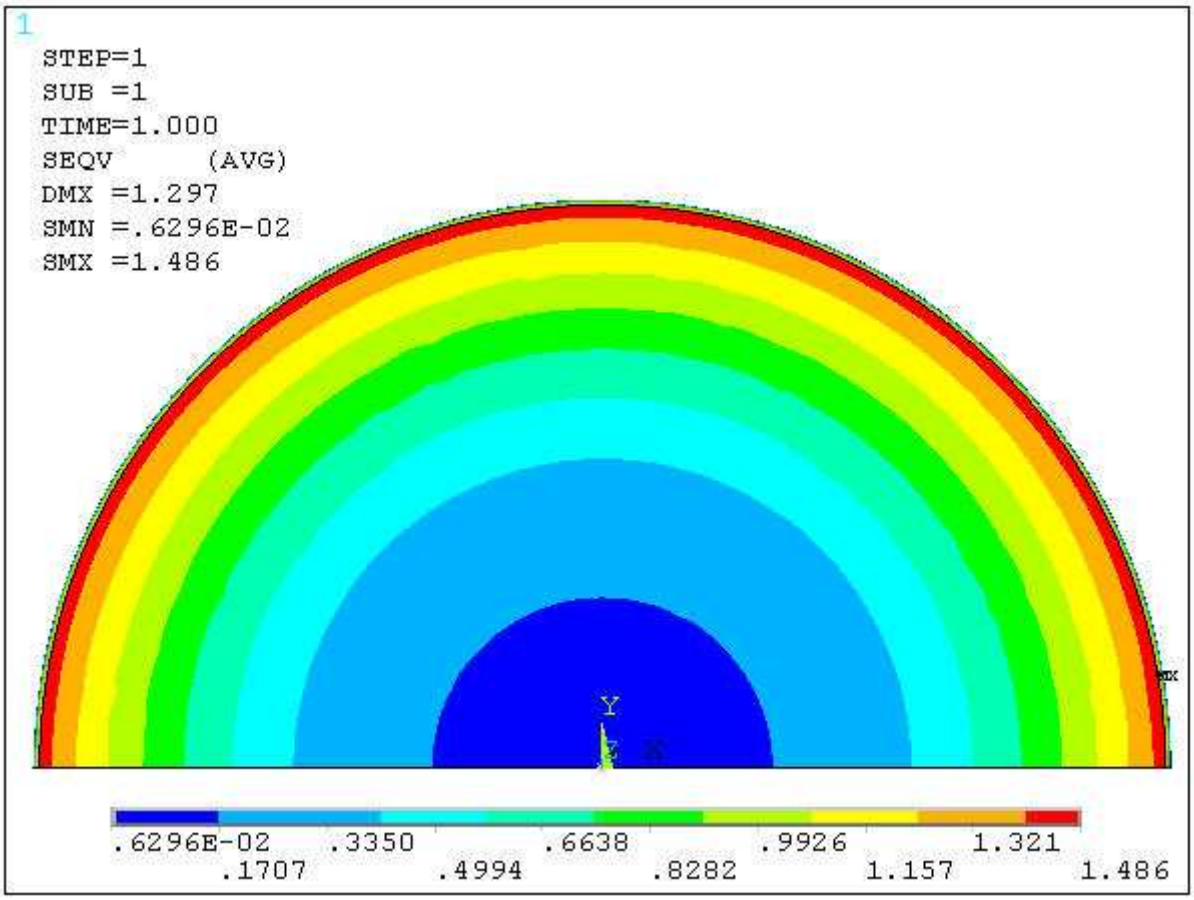

4.1 -sigma Von Mises (v. sections @100% Vmax)

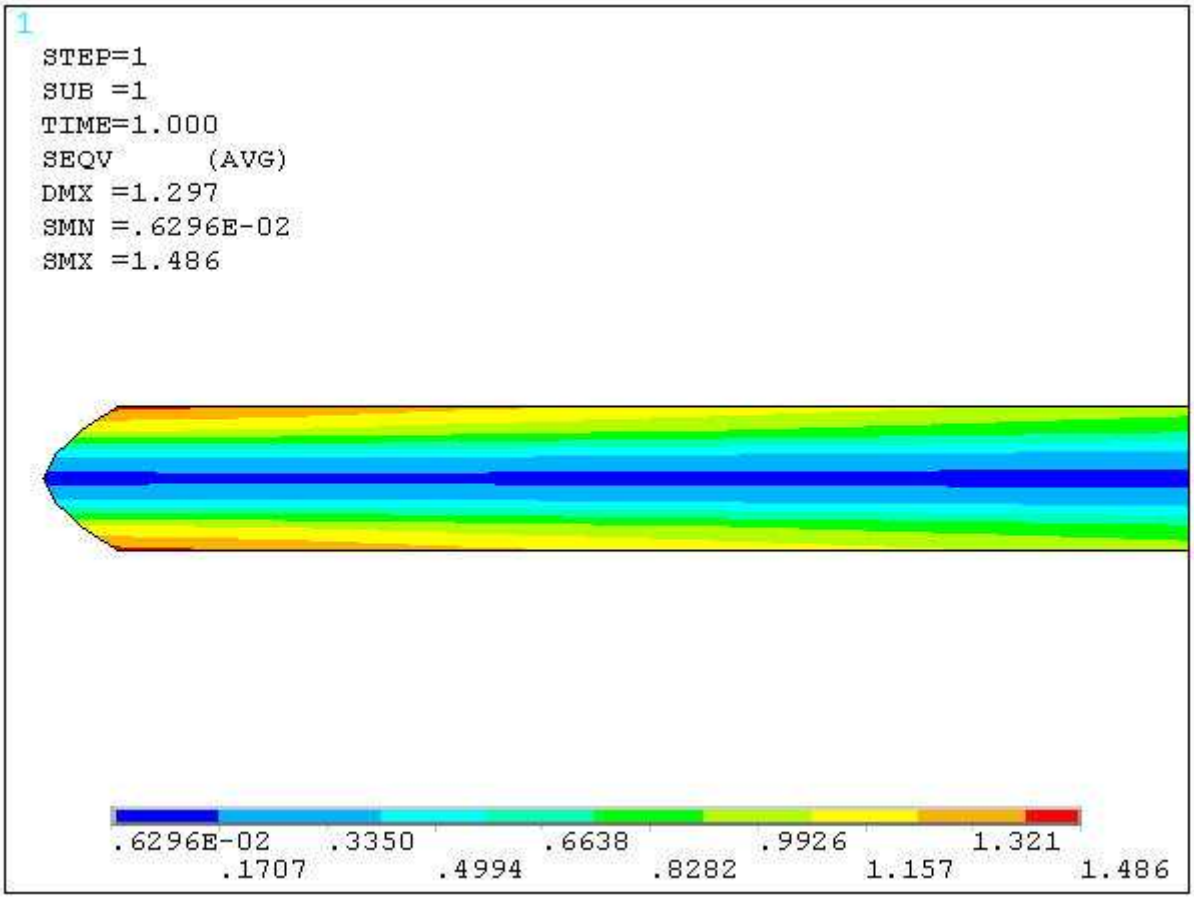

4.1 - deformad

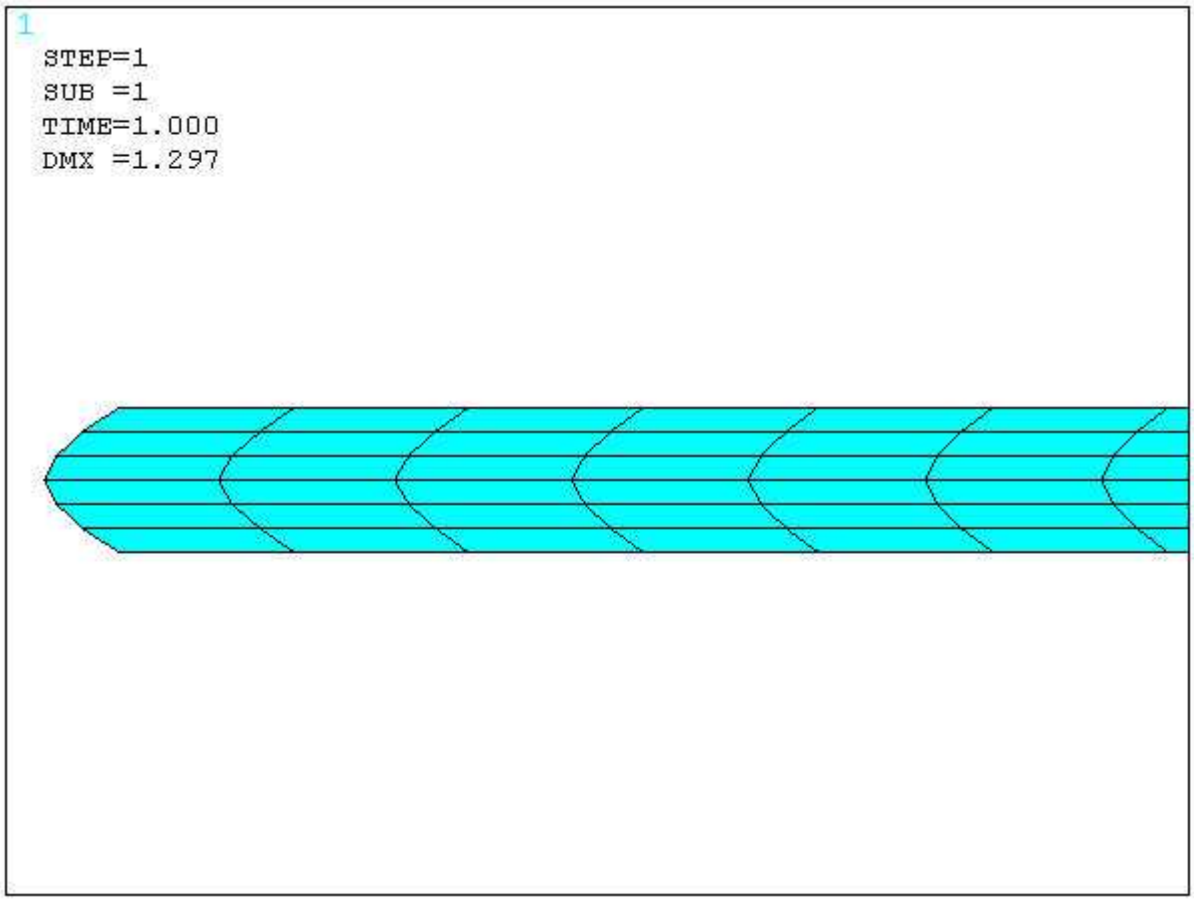
1
STEP=1
SUB =1
TIME=1.000
DMX =1.297

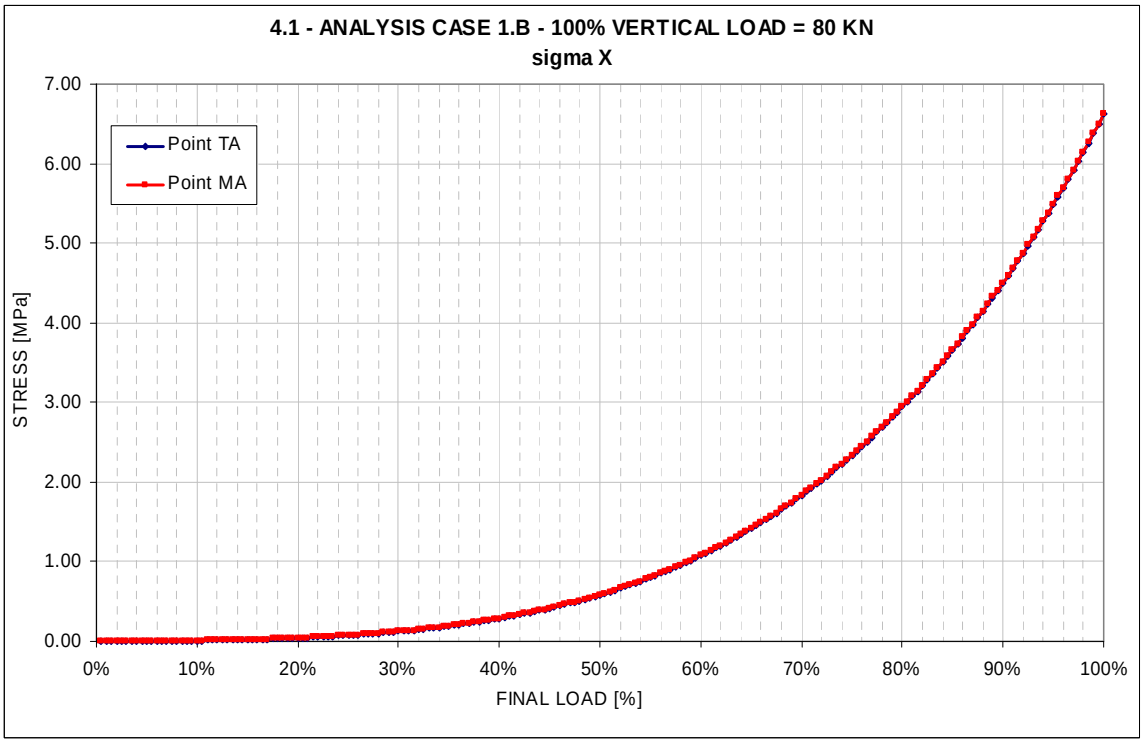
4.1 - ANALYSIS CASE 1.B - 100% VERTICAL LOAD = 80 KN
sigma X
Point TA
Point MA
STRESS [MPa]
7.00
6.00
5.00
4.00
3.00
2.00
1.00
0.00
0%
10%
20%
30%
40%
50%
60%
70%
80%
90%
100%
FINAL LOAD [%]

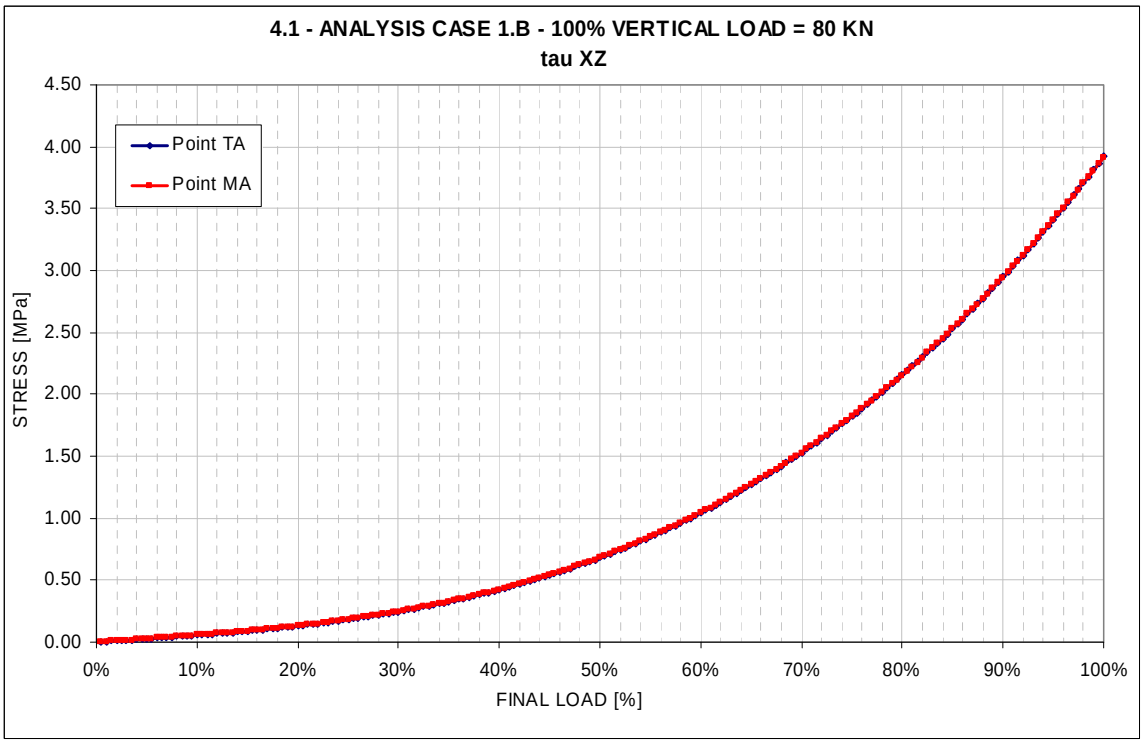
4.1 - ANALYSIS CASE 1.B - 100% VERTICAL LOAD = 80 KN
tau XZ
Point TA
Point MA
STRESS [MPa]
4.50
4.00
3.50
3.00
2.50
2.00
1.50
1.00
0.50
0.00
0%
10%
20%
30%
40%
50%
60%
70%
80%
90%
100%
FINAL LOAD [%]

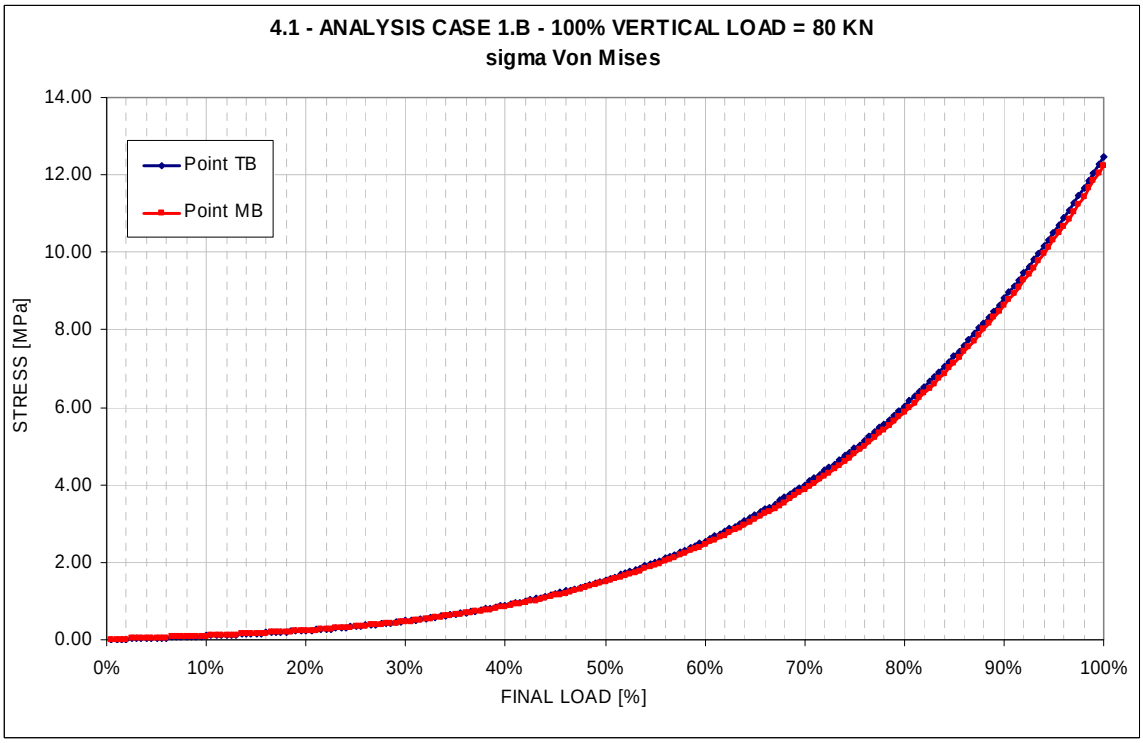
4.1 - ANALYSIS CASE 1.B - 100% VERTICAL LOAD = 80 KN
sigma Von Mises
Point TB
Point MB
STRESS [MPa]
14.00
12.00
10.00
8.00
6.00
4.00
2.00
0.00
0%
10%
20%
30%
40%
50%
60%
70%
80%
90%
100%
FINAL LOAD [%]

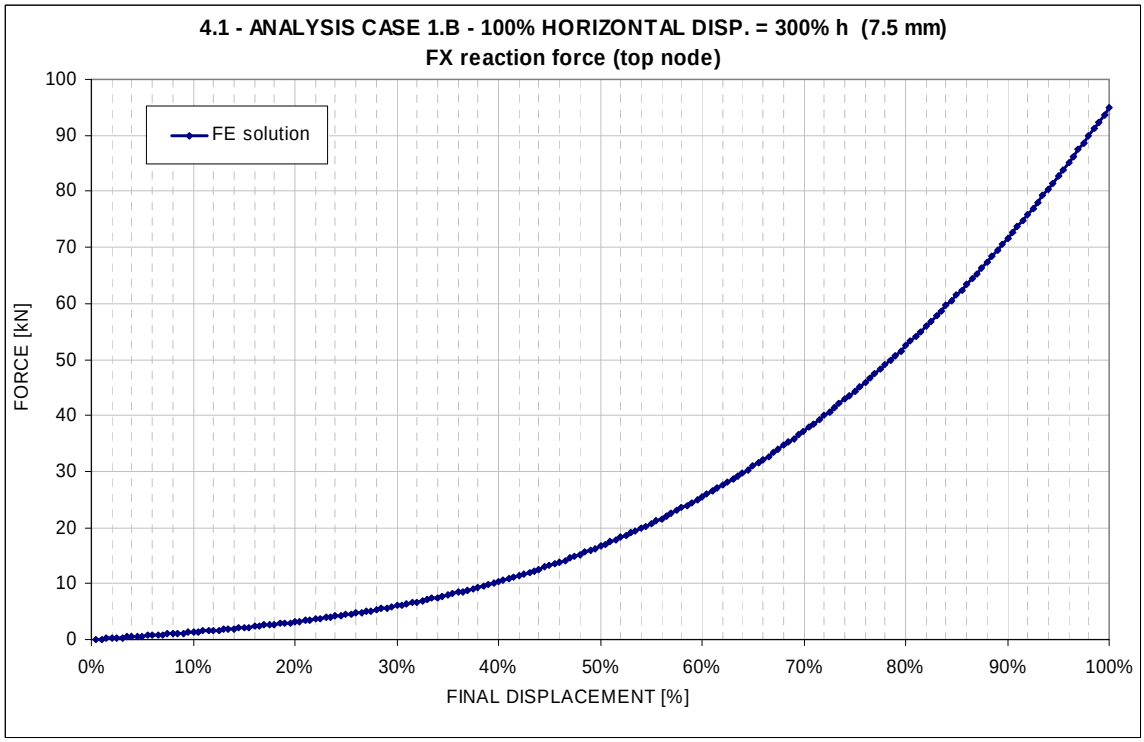
4.1 - ANALYSIS CASE 1.B - 100% HORIZONTAL DISP. = 300% h (7.5 mm)
FX reaction force (top node)
FE solution
FORCE [kN]
100
90
80
70
60
50
40
30
20
10
0
0%
10%
20%
30%
40%
50%
60%
70%
80%
90%
100%
FINAL DISPLACEMENT [%]

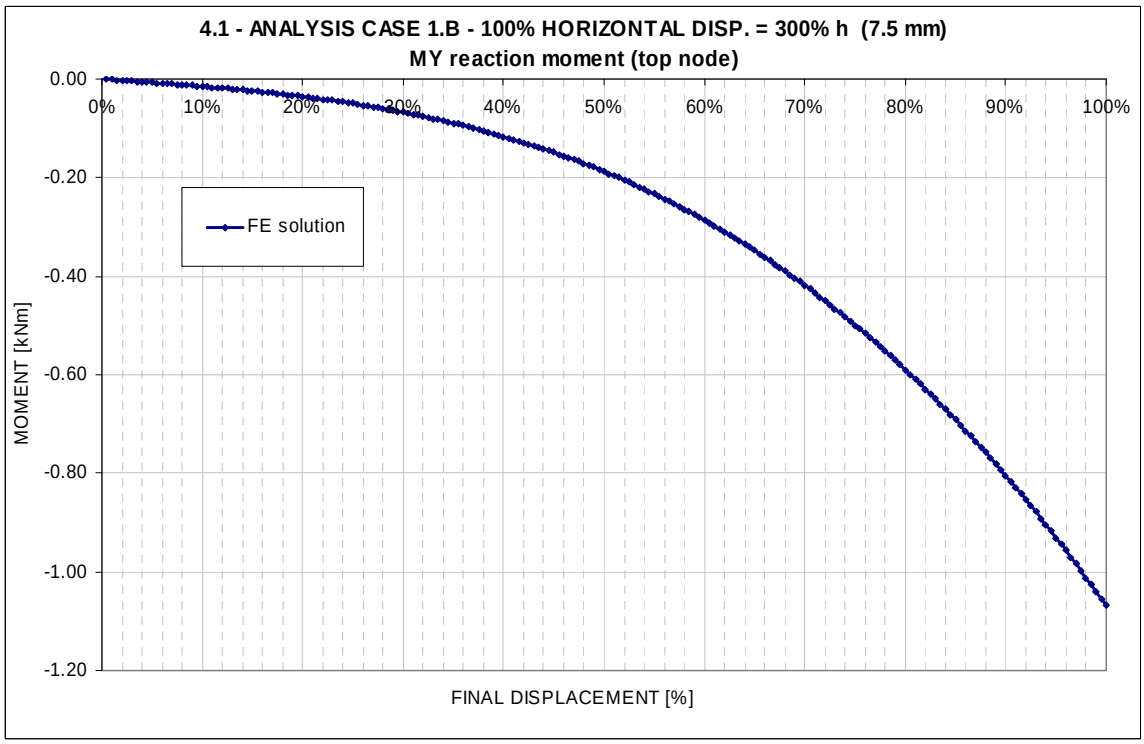
4.1 - ANALYSIS CASE 1.B - 100% HORIZONTAL DISP. = 300% h (7.5 mm)
MY reaction moment (top node)
FE solution
MOMENT [kNm]
0.00
-0.20
-0.40
-0.60
-0.80
-1.00
-1.20
0%
10%
20%
30%
40%
50%
60%
70%
80%
90%
100%
FINAL DISPLACEMENT [%]

4.2 - sigma x (2x h. top sections @150%,300% Hmax)

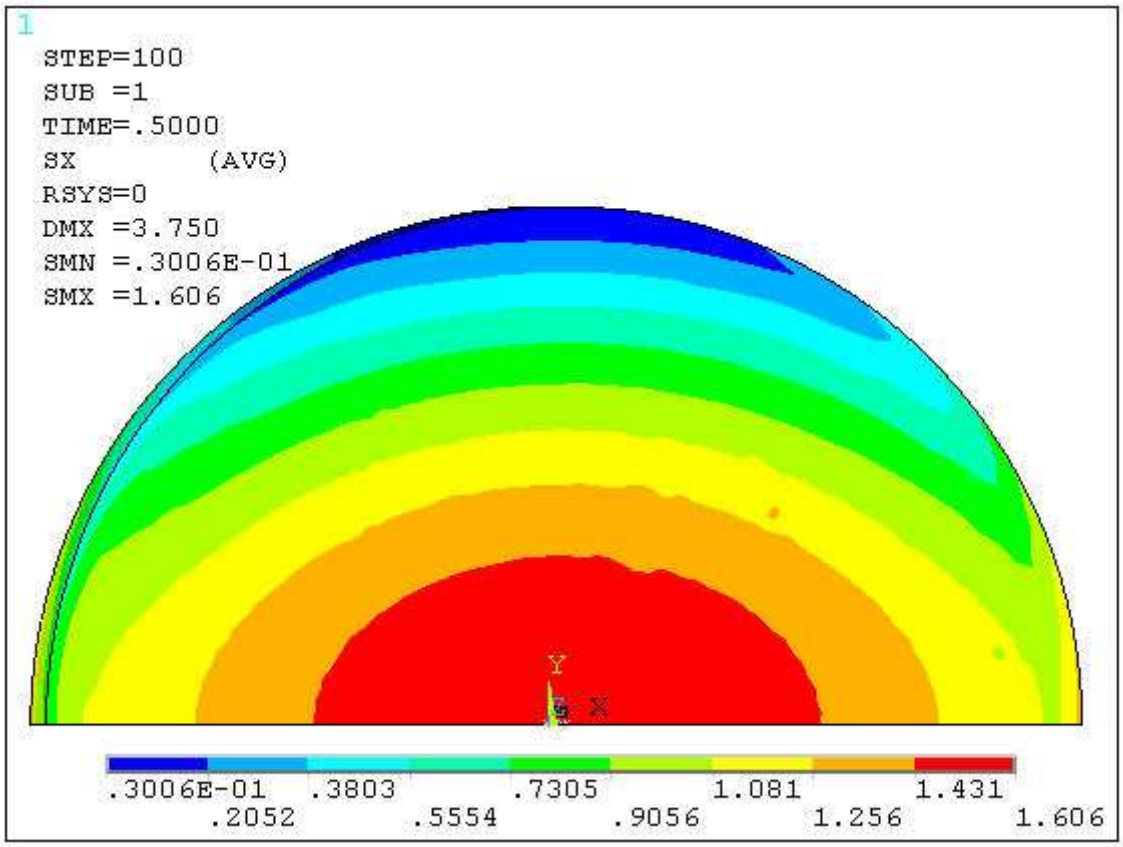

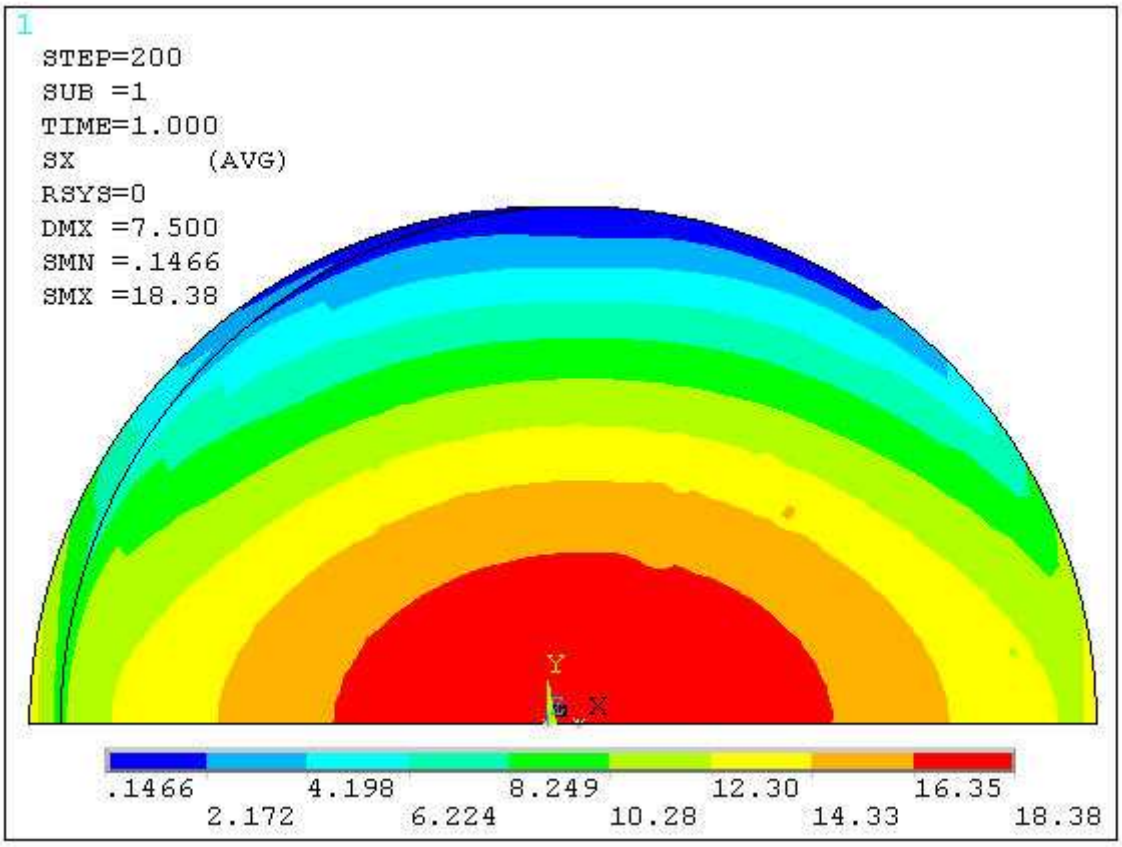

4.2 - sigma x(2x v. sections @150%,300% Hmax)

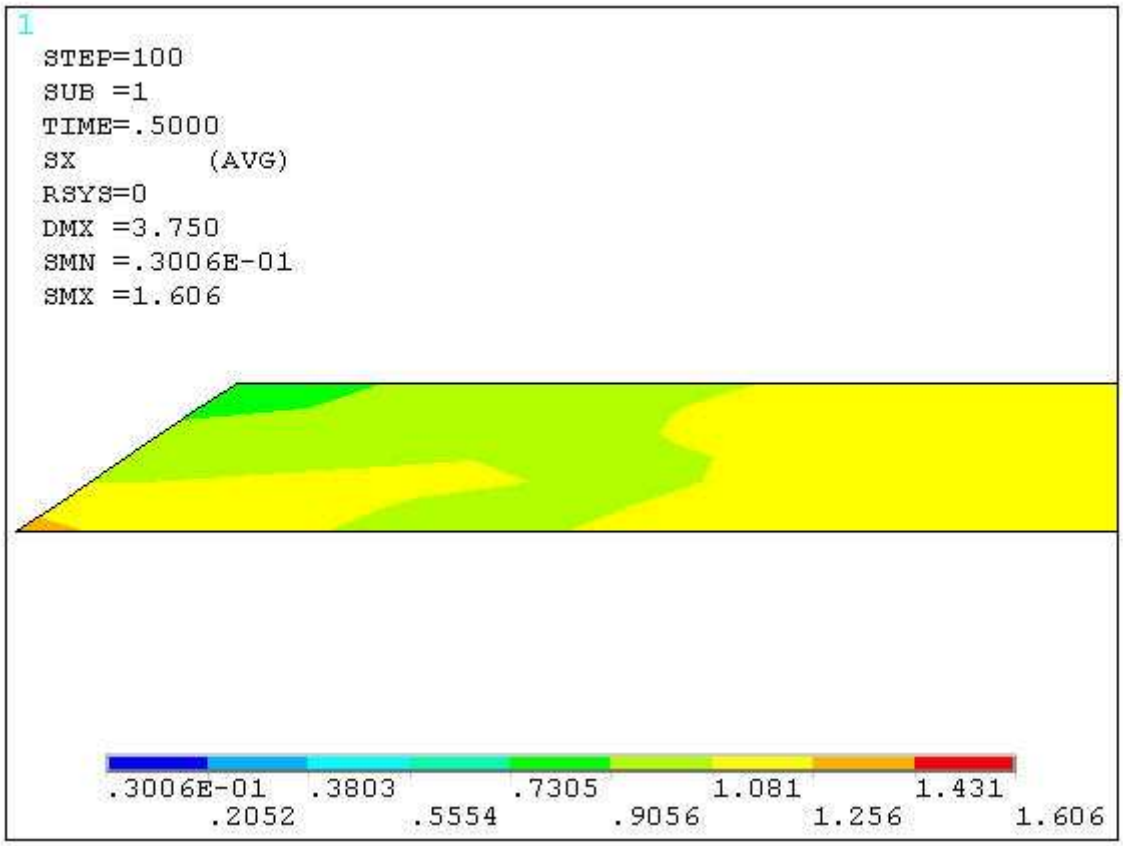

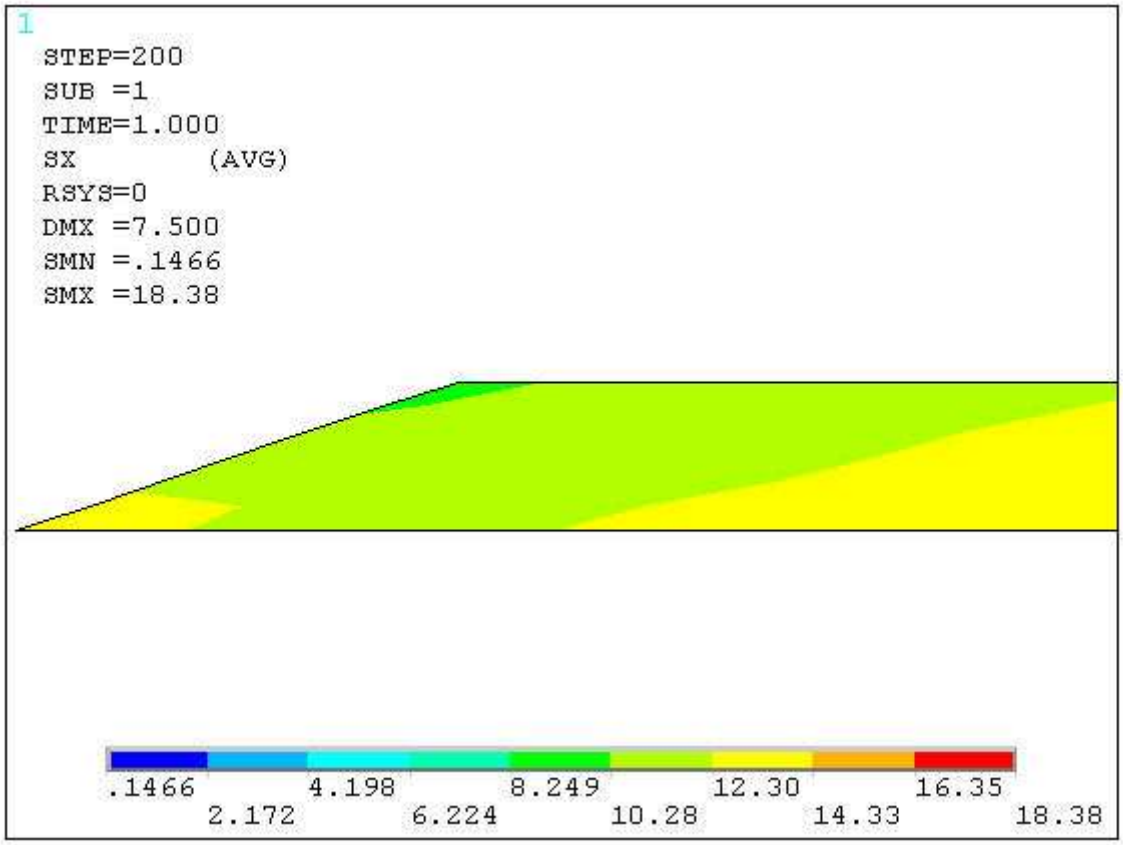

4.2 - tau zx (2x h. top sections @150%,300% Hmax)

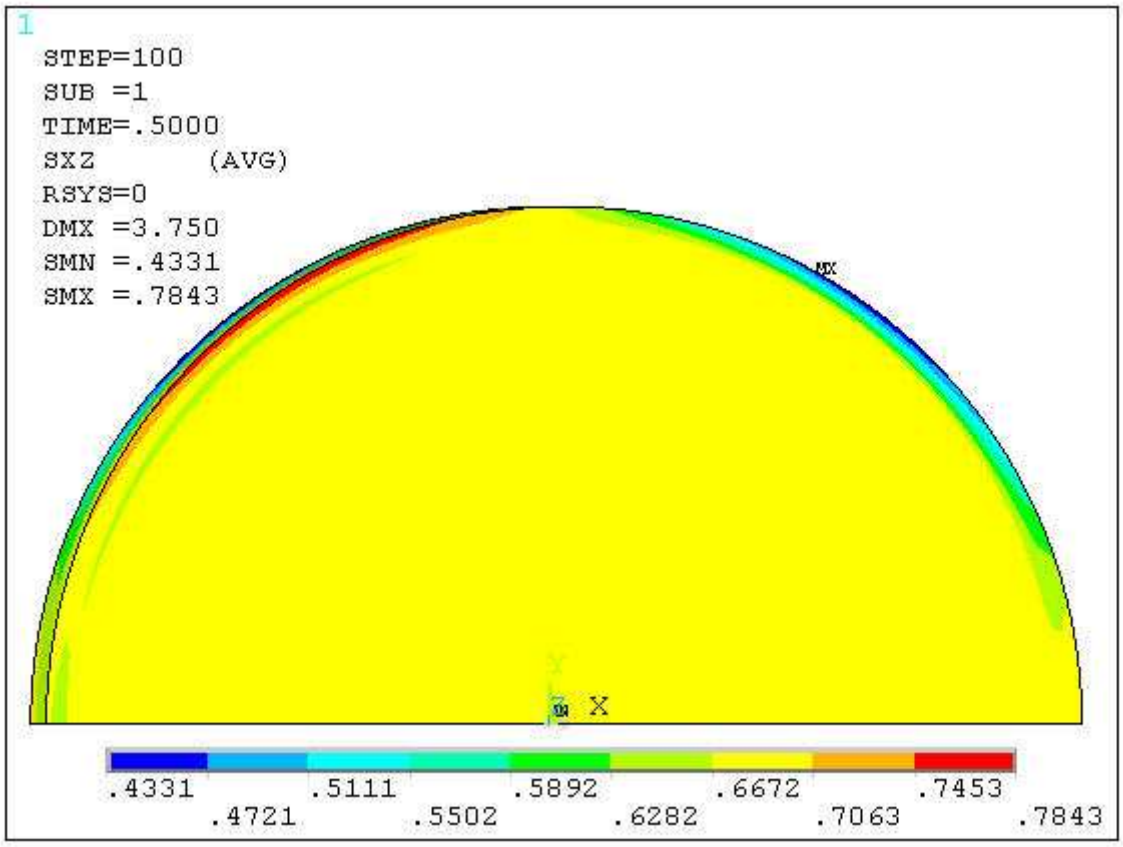

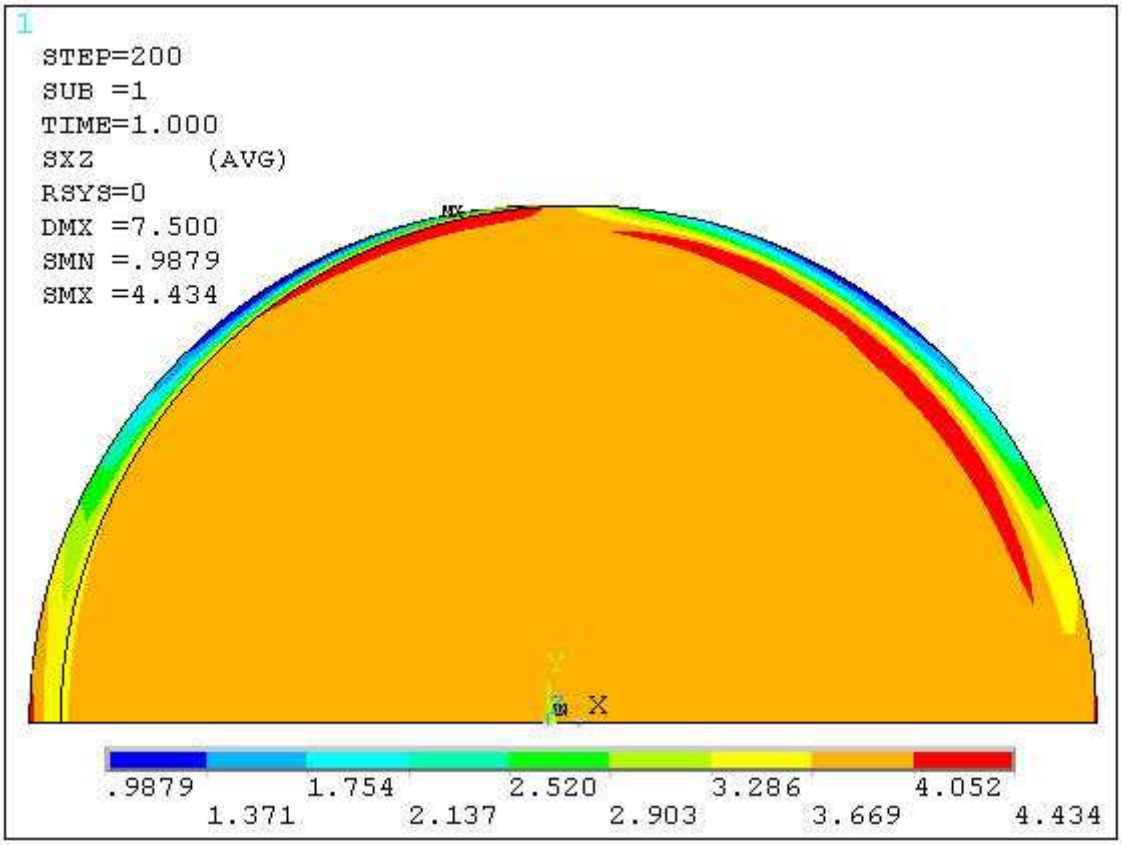

4.2 - tau zx (2x v. sections @150%,300% Hmax)

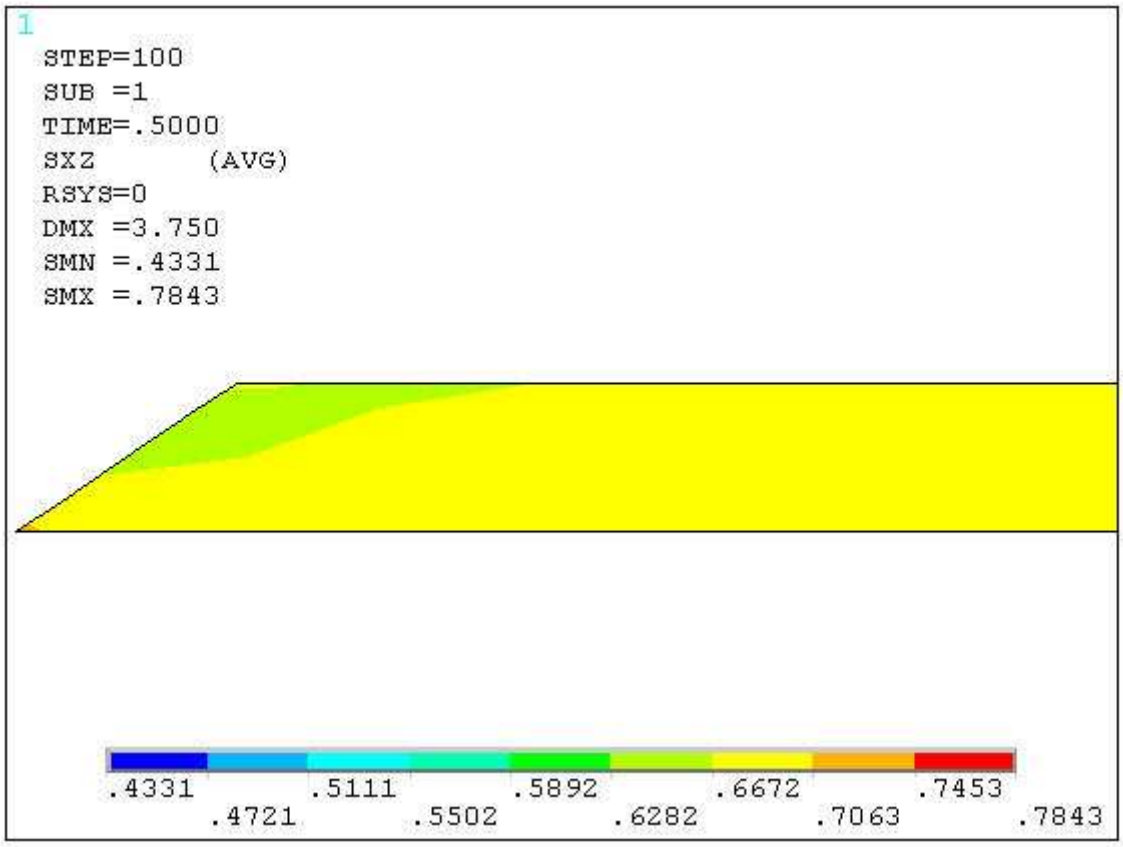

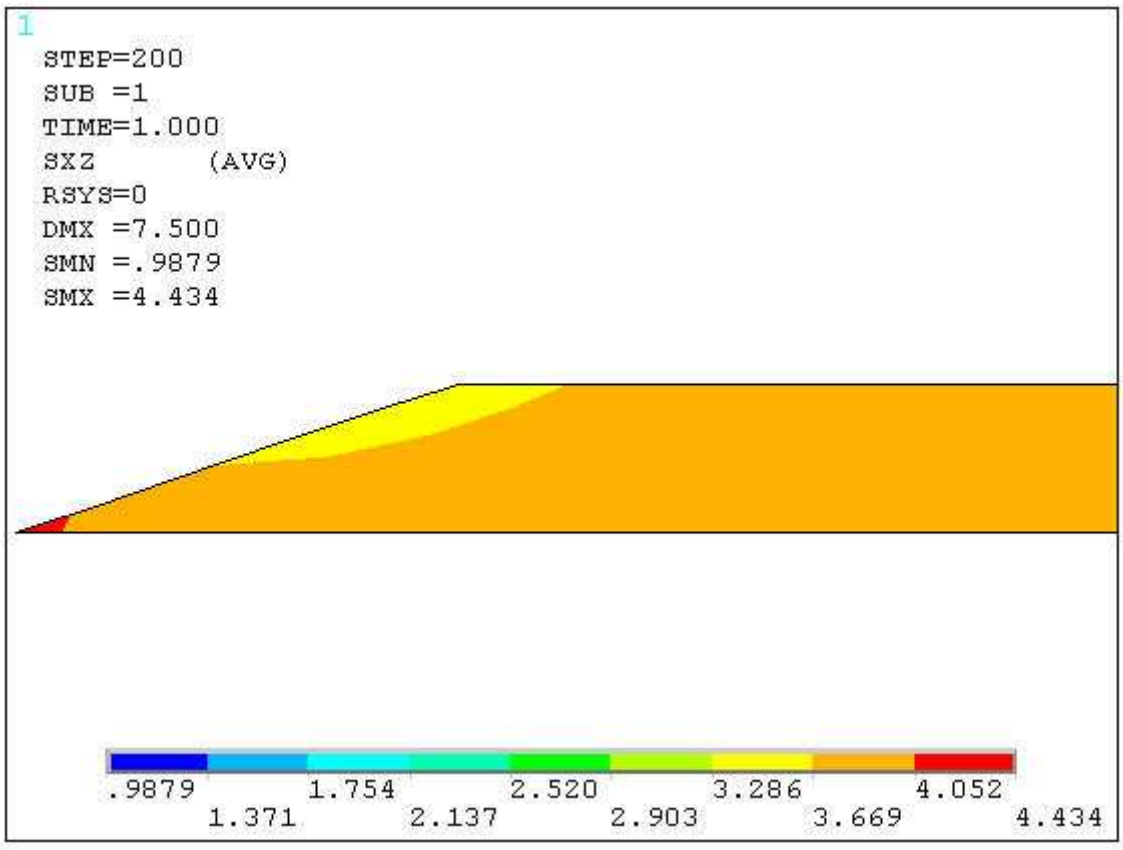

4.2 - sigma Von Mises (2x h. top sections @150%,300% Hmax)

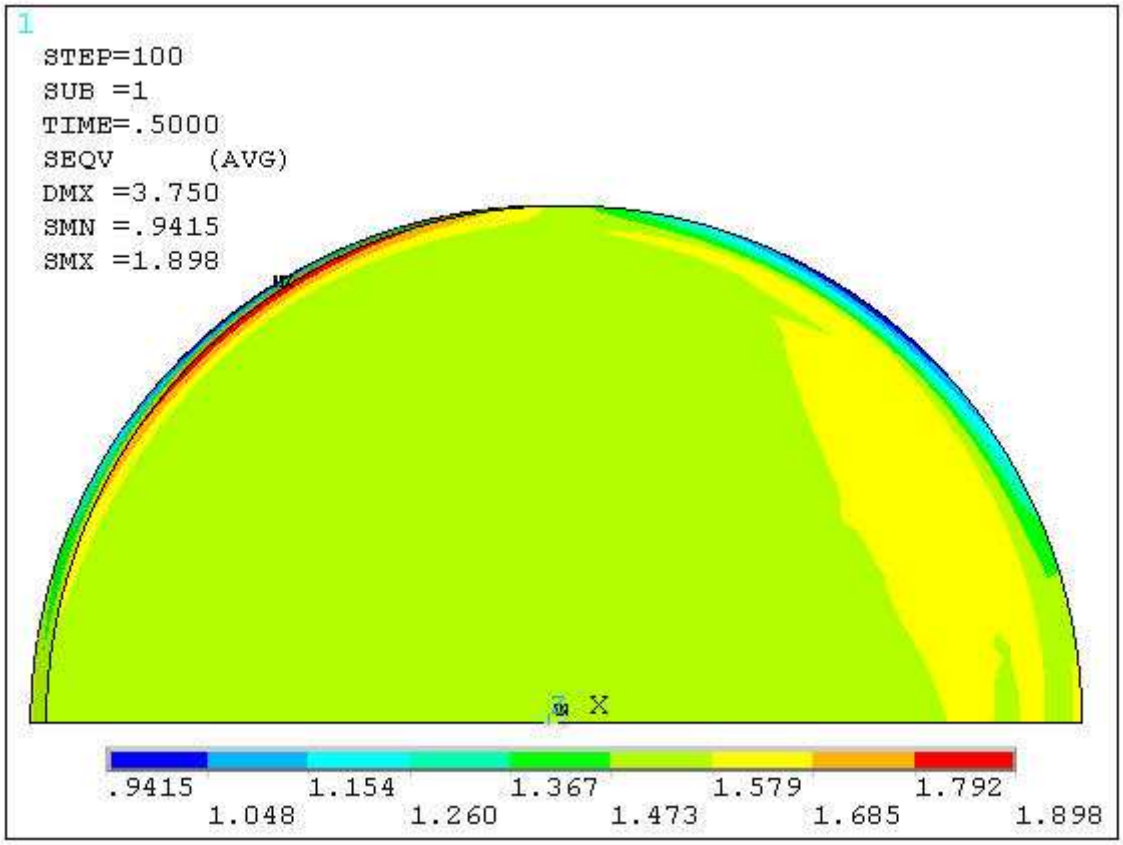

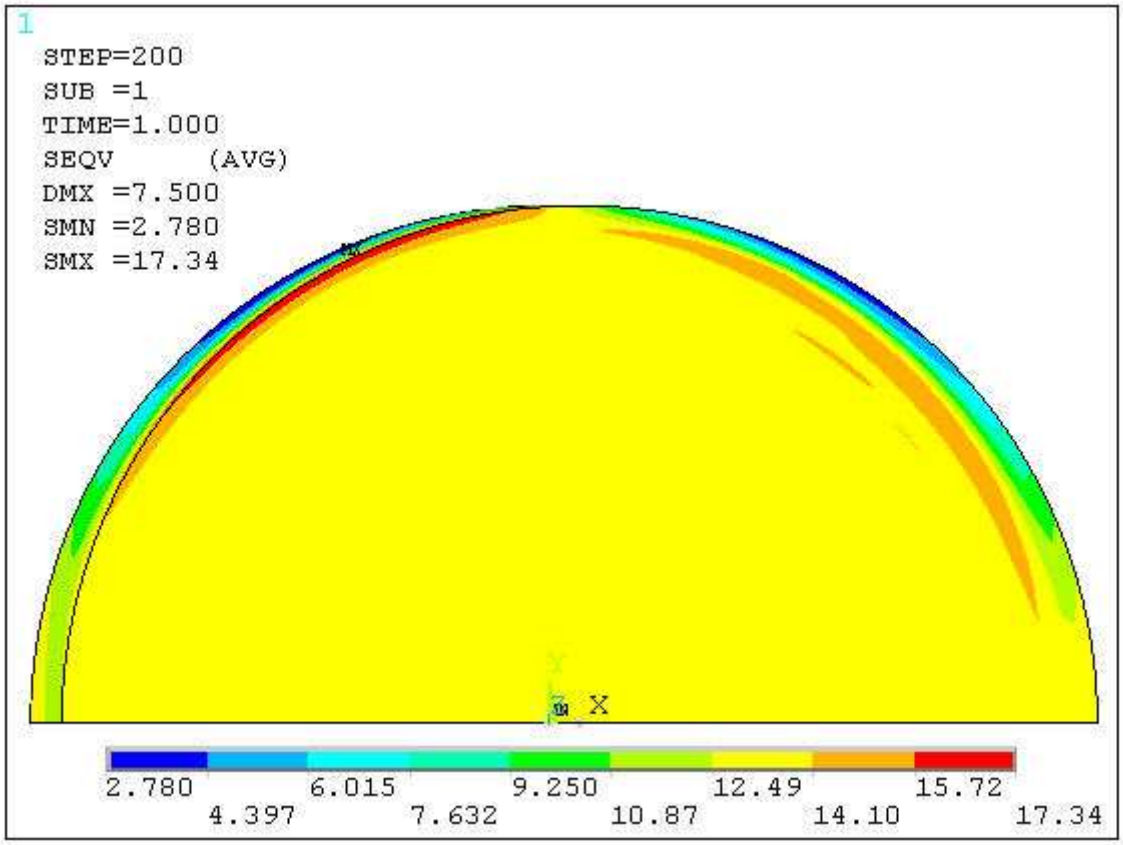

4.2 - sigma Von Mises (2x v. sections @150%,300% Hmax)

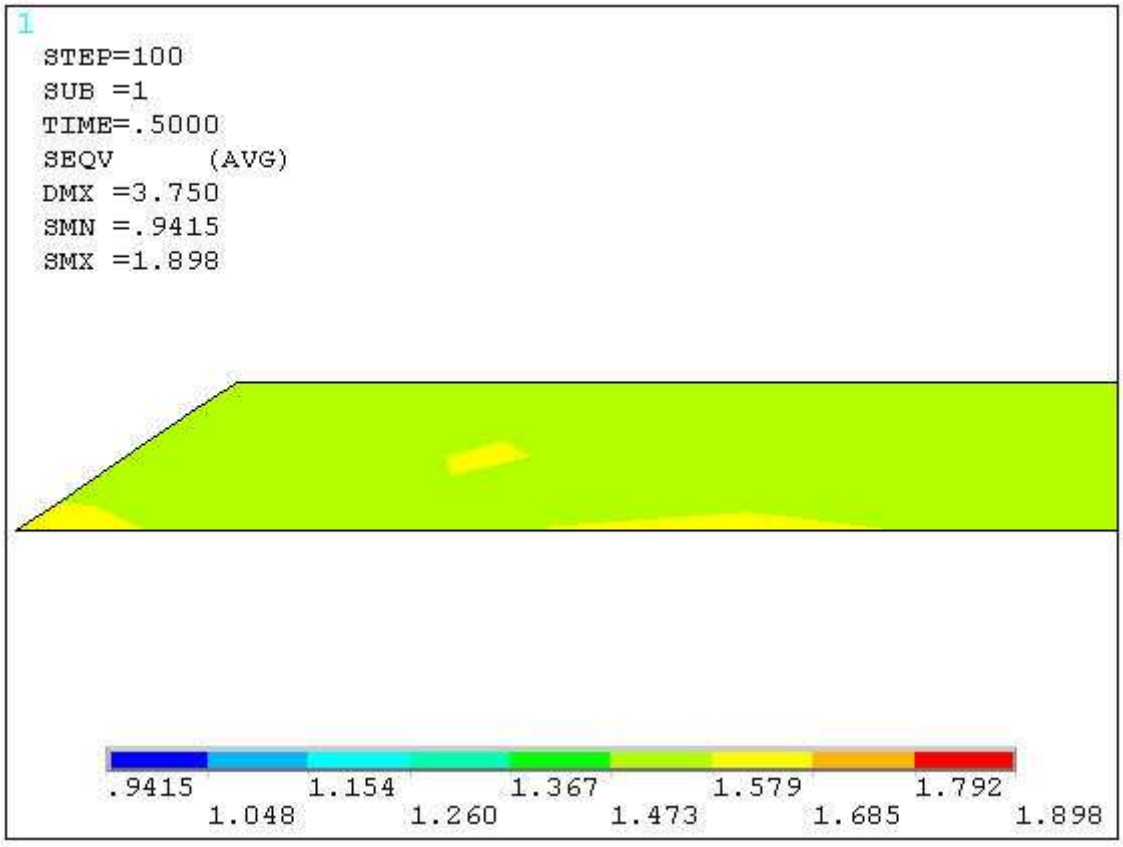

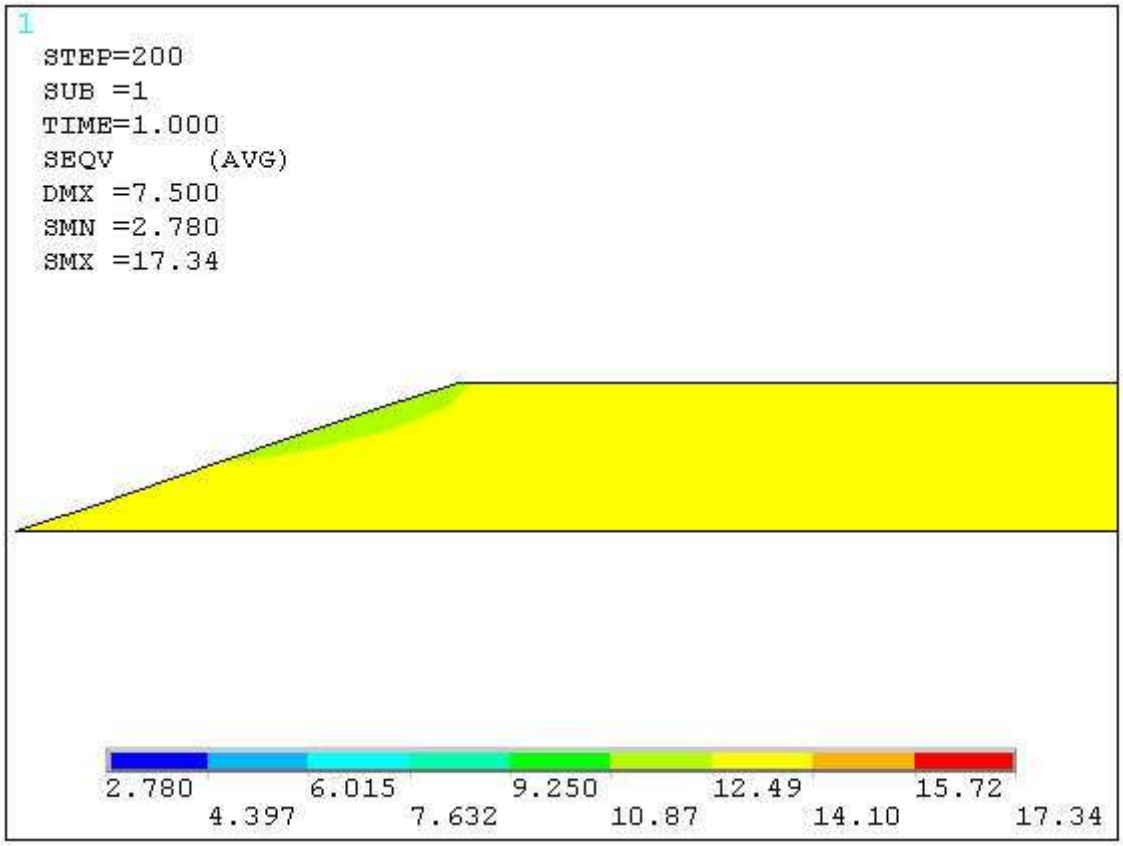

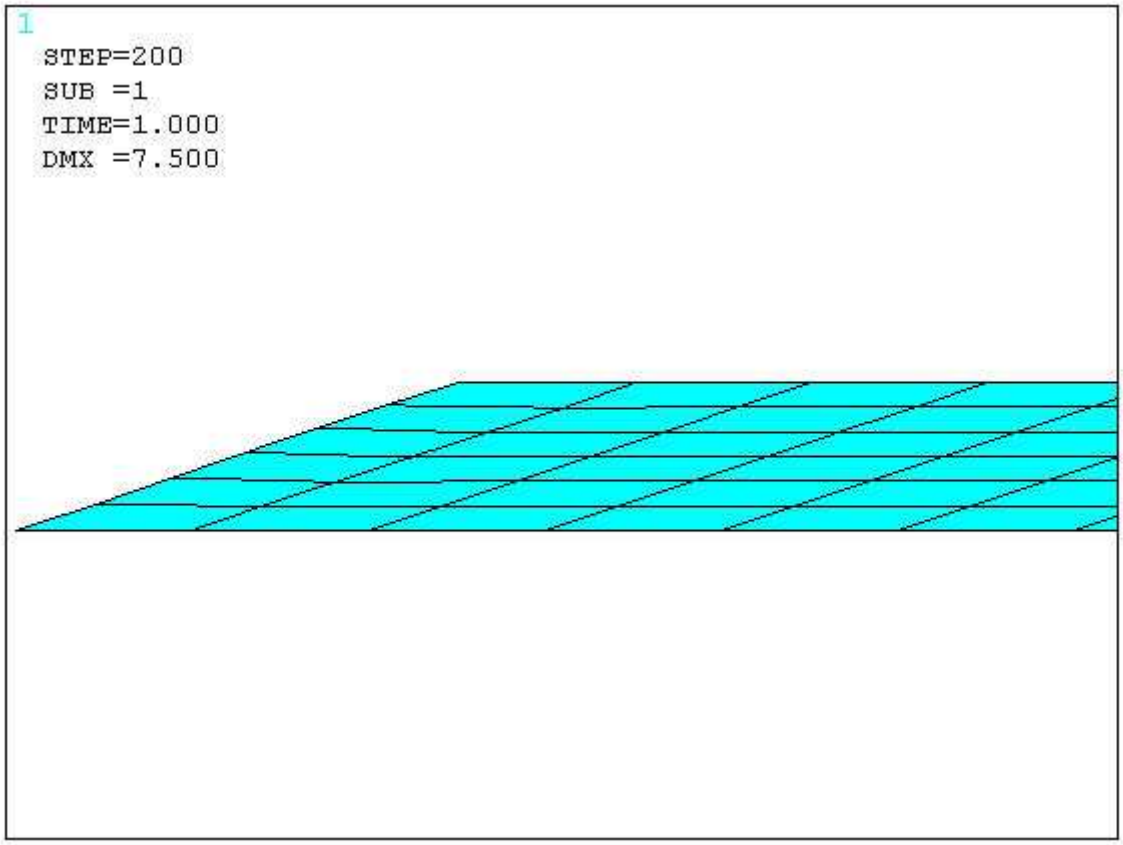
1
STEP=200
SUB =1
TIME=1.000
DMX =7.500

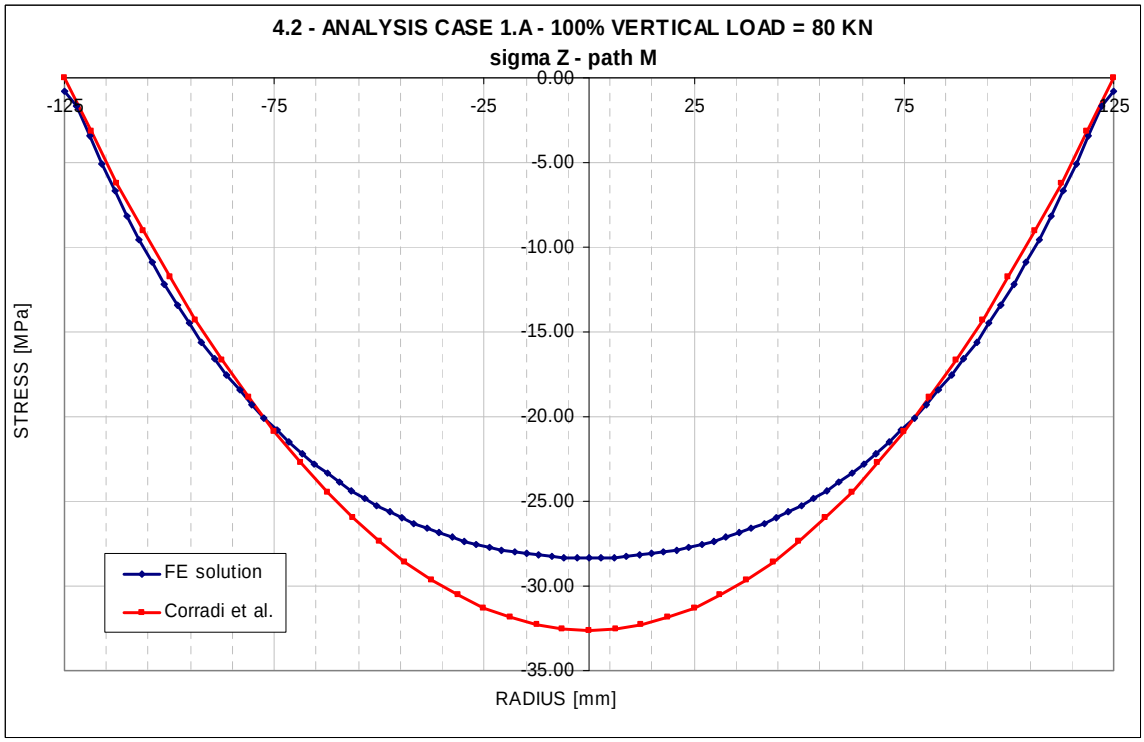
4.2 - ANALYSIS CASE 1.A - 100% VERTICAL LOAD = 80 KN
sigma Z - path M
0.00
-5.00
-10.00
-15.00
-20.00
-25.00
-30.00
-35.00
-125
-75
-25
25
75
125
STRESS [MPa]
RADIUS [mm]
FE solution
Corradi et al.

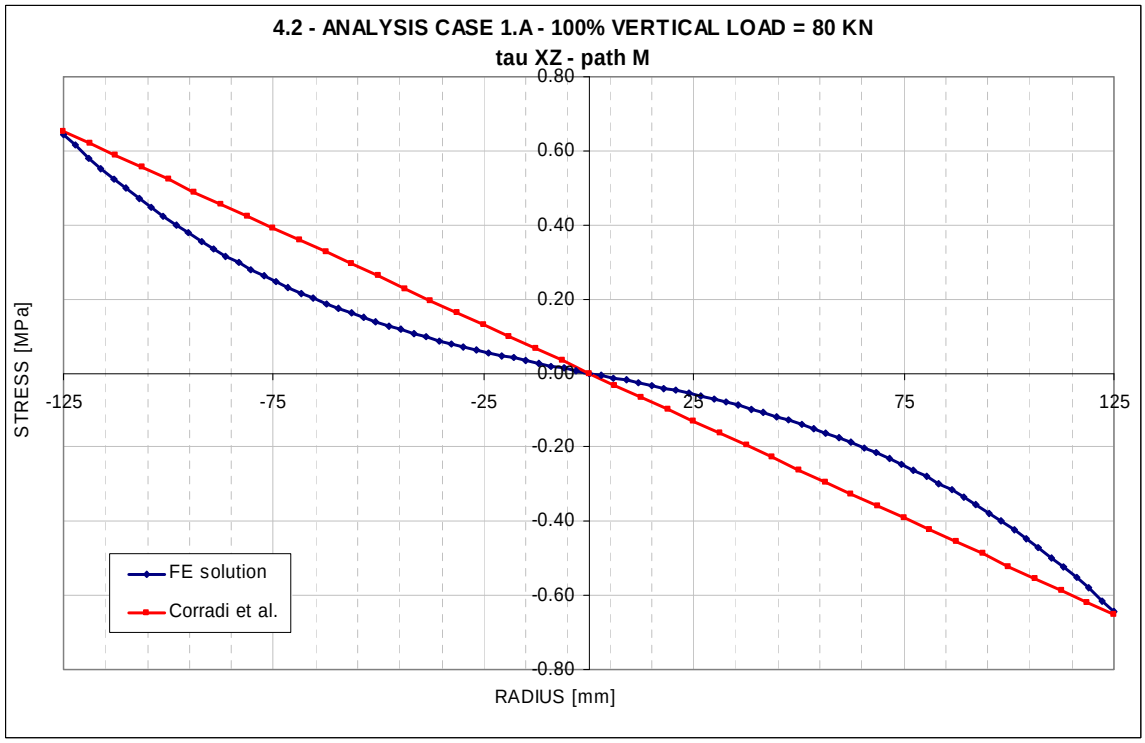
4.2 - ANALYSIS CASE 1.A - 100% VERTICAL LOAD = 80 KN
tau XZ - path M
0.80
0.60
0.40
0.20
0.00
-0.20
-0.40
-0.60
-0.80
-125
-75
-25
25
75
125
STRESS [MPa]
RADIUS [mm]
FE solution
Corradi et al.

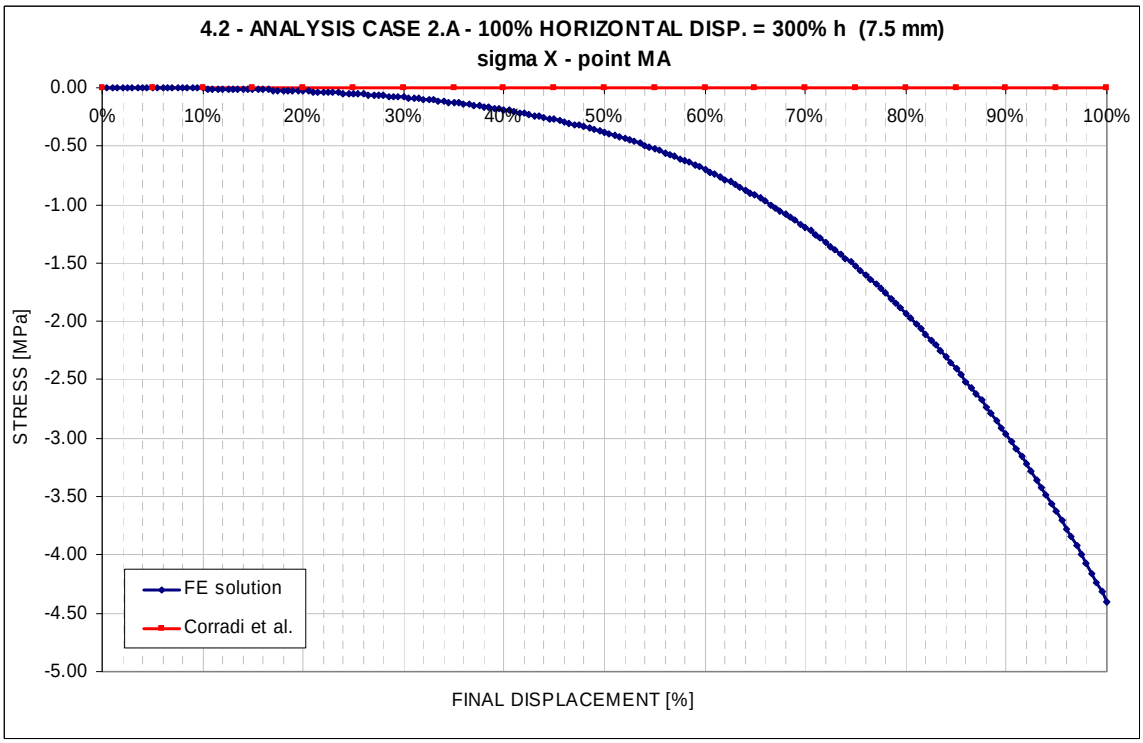
4.2 - ANALYSIS CASE 2.A - 100% HORIZONTAL DISP. = 300% h (7.5 mm)
sigma X - point MA
STRESS [MPa]
0.00
-0.50
-1.00
-1.50
-2.00
-2.50
-3.00
-3.50
-4.00
-4.50
-5.00
0%
10%
20%
30%
40%
50%
60%
70%
80%
90%
100%
FE solution
Corradi et al.
FINAL DISPLACEMENT [%]

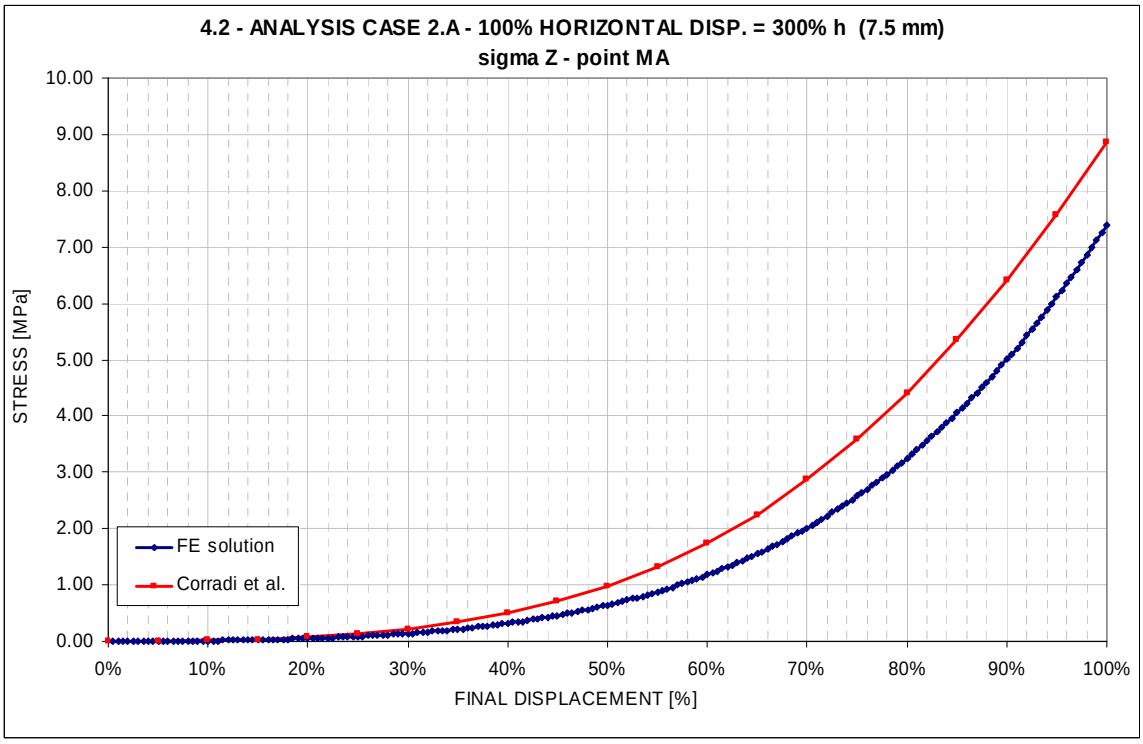
4.2 - ANALYSIS CASE 2.A - 100% HORIZONTAL DISP. = 300% h (7.5 mm)
sigma Z - point MA
STRESS [MPa]
10.00
9.00
8.00
7.00
6.00
5.00
4.00
3.00
2.00
1.00
0.00
0%
10%
20%
30%
40%
50%
60%
70%
80%
90%
100%
FE solution
Corradi et al.
FINAL DISPLACEMENT [%]

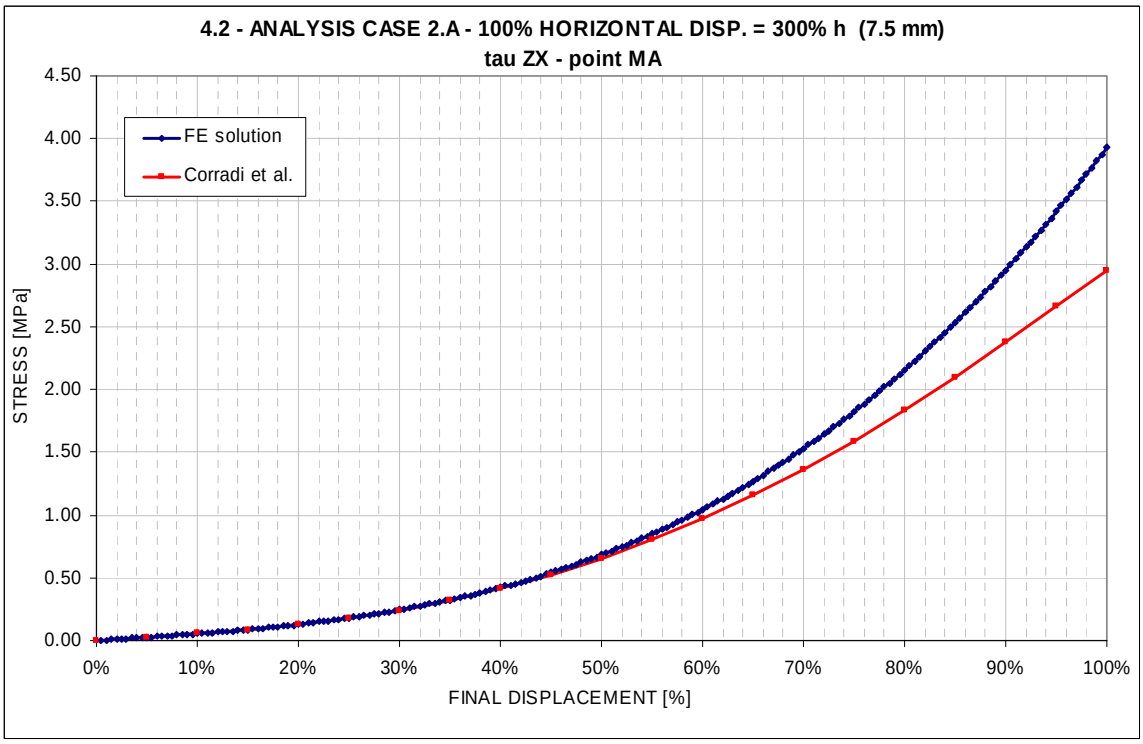
4.2 - ANALYSIS CASE 2.A - 100% HORIZONTAL DISP. = 300% h (7.5 mm)
tau ZX - point MA
FE solution
Corradi et al.
STRESS [MPa]
FINAL DISPLACEMENT [%]
0.00
0.50
1.00
1.50
2.00
2.50
3.00
3.50
4.00
4.50
0%
10%
20%
30%
40%
50%
60%
70%
80%
90%
100%

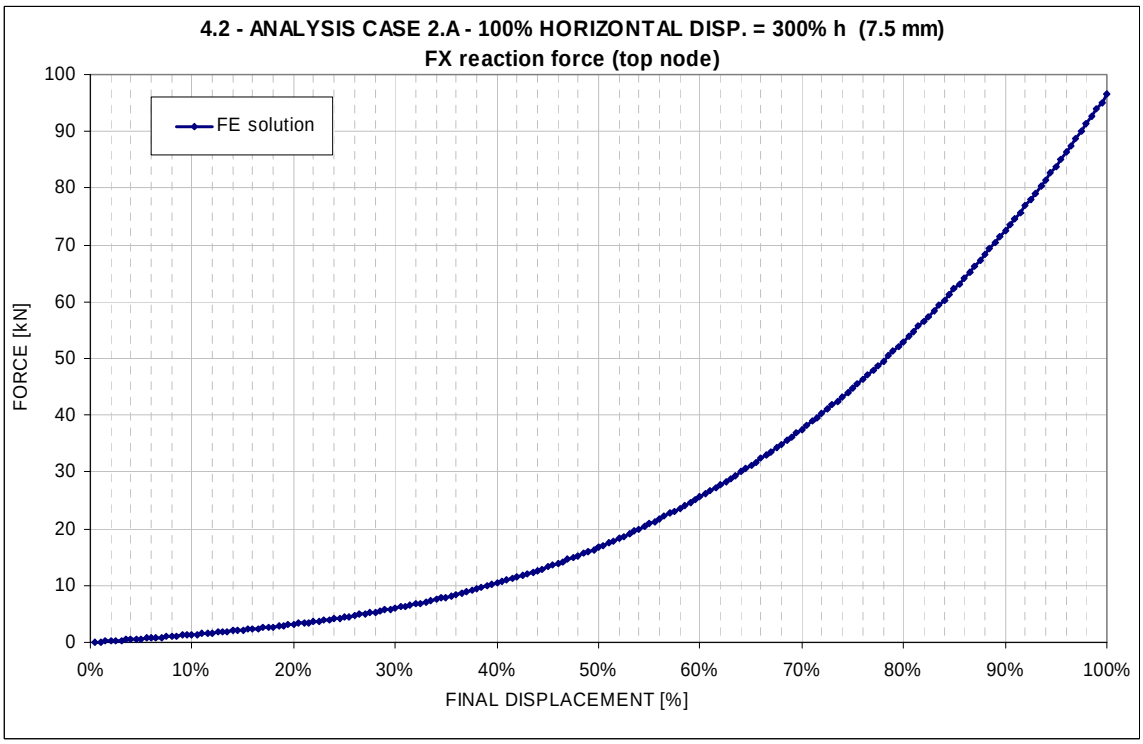
4.2 - ANALYSIS CASE 2.A - 100% HORIZONTAL DISP. = 300% h (7.5 mm)
FX reaction force (top node)
FE solution
FORCE [kN]
FINAL DISPLACEMENT [%]
0
10
20
30
40
50
60
70
80
90
100
0%
10%
20%
30%
40%
50%
60%
70%
80%
90%
100%

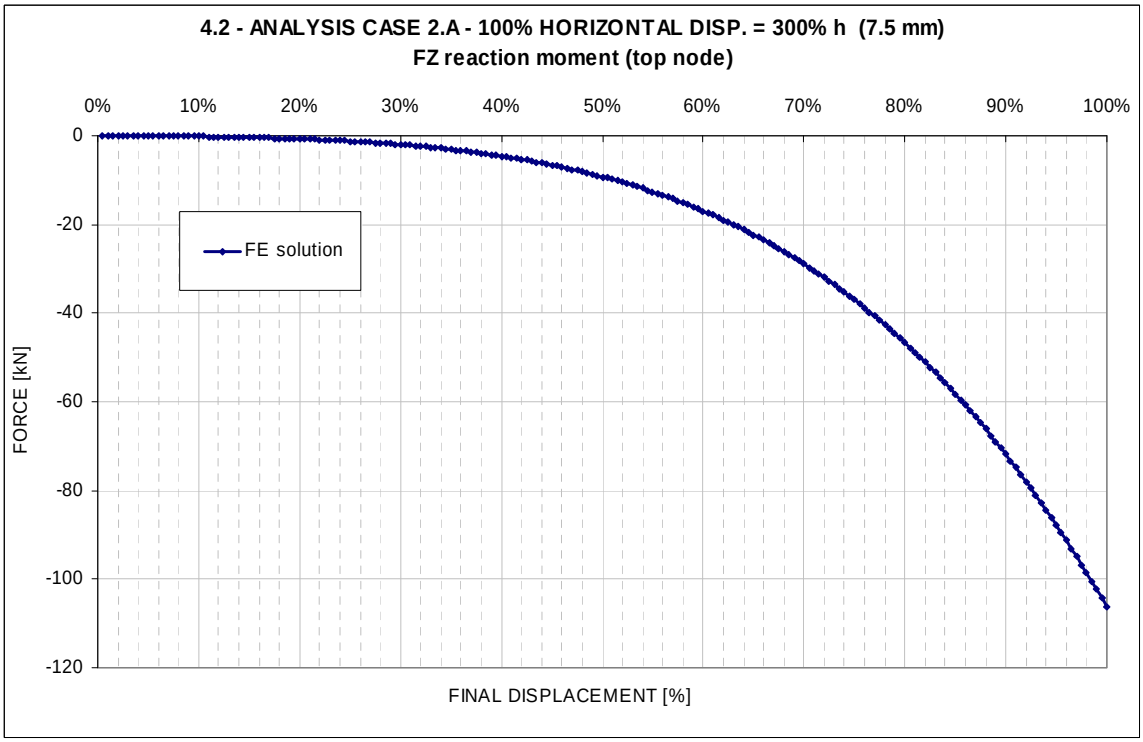
4.2 - ANALYSIS CASE 2.A - 100% HORIZONTAL DISP. = 300% h (7.5 mm)
FZ reaction moment (top node)
0%
10%
20%
30%
40%
50%
60%
70%
80%
90%
100%
0
-20
-40
-60
-80
-100
-120
FE solution
FORCE [kN]
FINAL DISPLACEMENT [%]

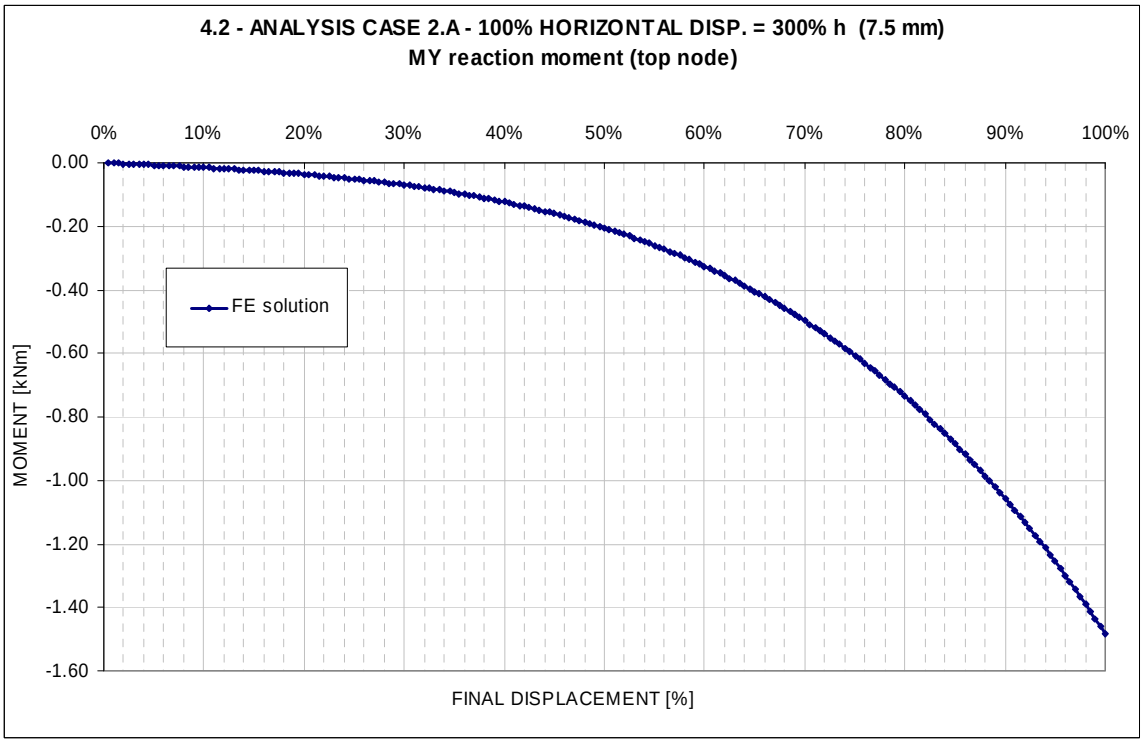
4.2 - ANALYSIS CASE 2.A - 100% HORIZONTAL DISP. = 300% h (7.5 mm)
MY reaction moment (top node)
0%
10%
20%
30%
40%
50%
60%
70%
80%
90%
100%
0.00
-0.20
-0.40
-0.60
-0.80
-1.00
-1.20
-1.40
-1.60
FE solution
MOMENT [kNm]
FINAL DISPLACEMENT [%]

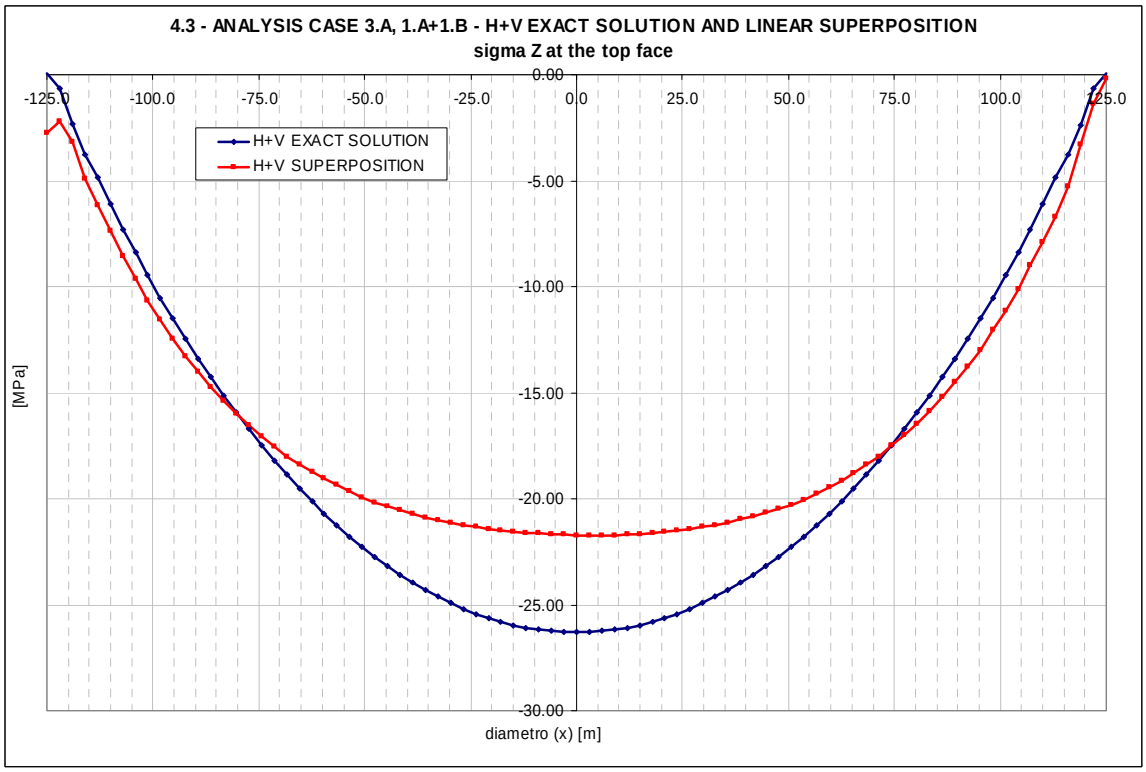
4.3 - ANALYSIS CASE 3.A, 1.A+1.B - H+V EXACT SOLUTION AND LINEAR SUPERPOSITION
sigma Z at the top face
H+V EXACT SOLUTION
H+V SUPERPOSITION
[MPa]
diametro (x) [m]
0.00
-5.00
-10.00
-15.00
-20.00
-25.00
-30.00
-125.0
-100.0
-75.0
-50.0
-25.0
0.0
25.0
50.0
75.0
100.0
125.0

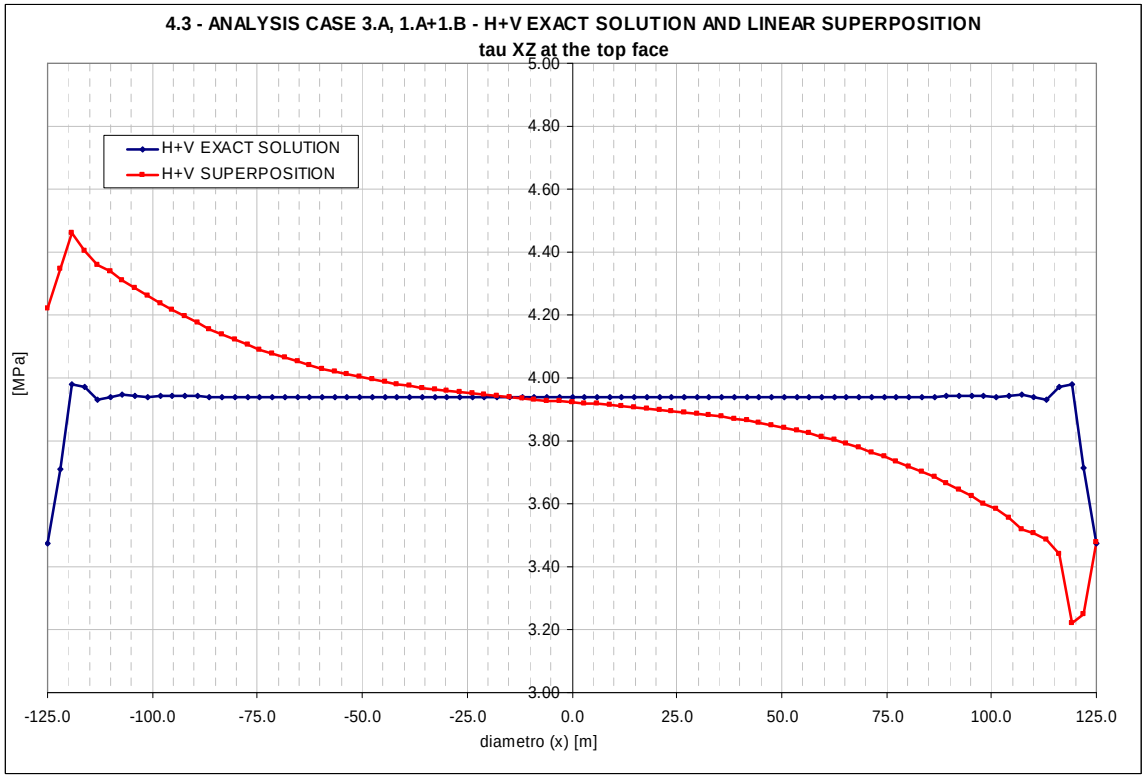
4.3 - ANALYSIS CASE 3.A, 1.A+1.B - H+V EXACT SOLUTION AND LINEAR SUPERPOSITION
tau XZ at the top face
H+V EXACT SOLUTION
H+V SUPERPOSITION
[MPa]
diametro (x) [m]
5.00
4.80
4.60
4.40
4.20
4.00
3.80
3.60
3.40
3.20
3.00
-125.0
-100.0
-75.0
-50.0
-25.0
0.0
25.0
50.0
75.0
100.0
125.0

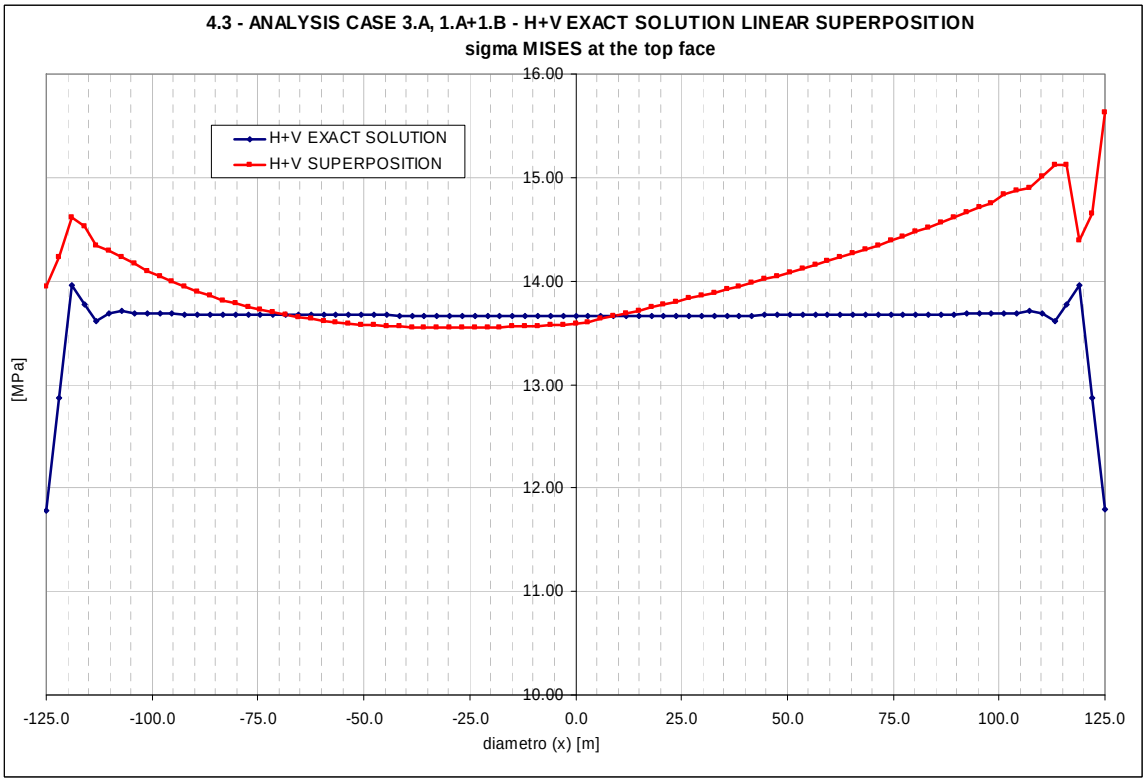
4.3 - ANALYSIS CASE 3.A, 1.A+1.B - H+V EXACT SOLUTION LINEAR SUPERPOSITION
sigma MISES at the top face
H+V EXACT SOLUTION
H+V SUPERPOSITION
[MPa]
16.00
15.00
14.00
13.00
12.00
11.00
10.00
-125.0
-100.0
-75.0
-50.0
-25.0
0.0
25.0
50.0
75.0
100.0
125.0
diametro (x) [m]

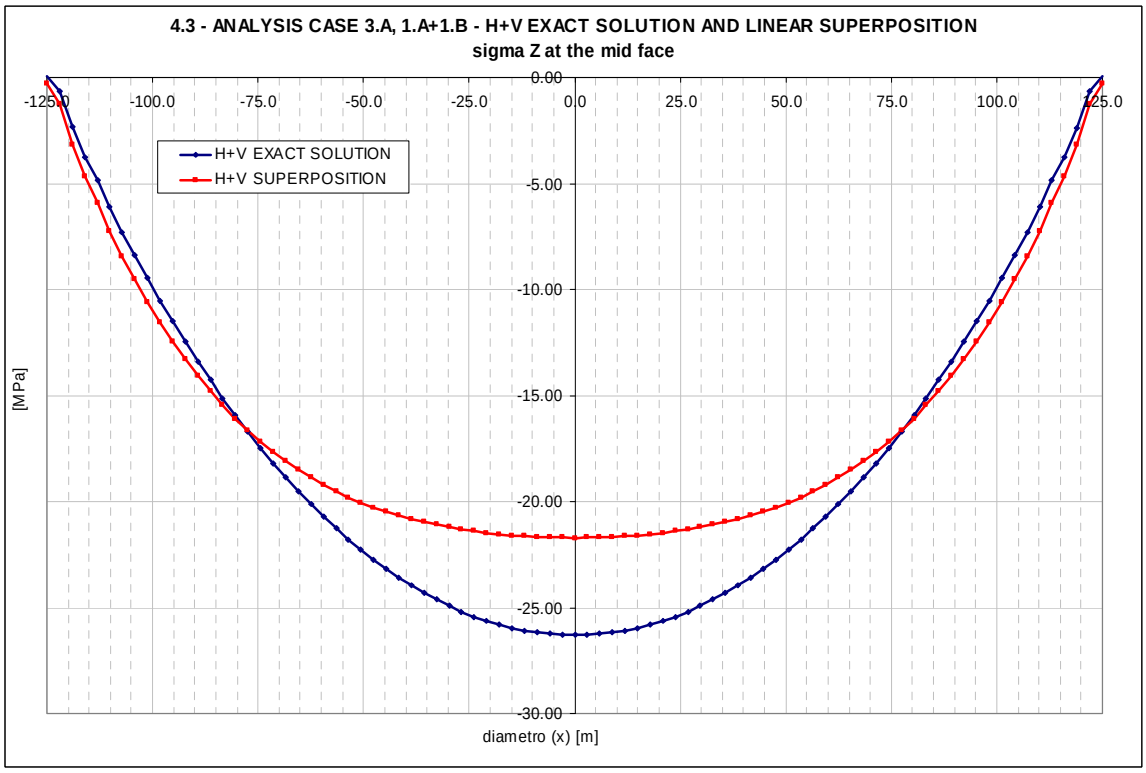
4.3 - ANALYSIS CASE 3.A, 1.A+1.B - H+V EXACT SOLUTION AND LINEAR SUPERPOSITION
sigma Z at the mid face
H+V EXACT SOLUTION
H+V SUPERPOSITION
[MPa]
0.00
-5.00
-10.00
-15.00
-20.00
-25.00
-30.00
-125.0
-100.0
-75.0
-50.0
-25.0
0.0
25.0
50.0
75.0
100.0
125.0
diametro (x) [m]

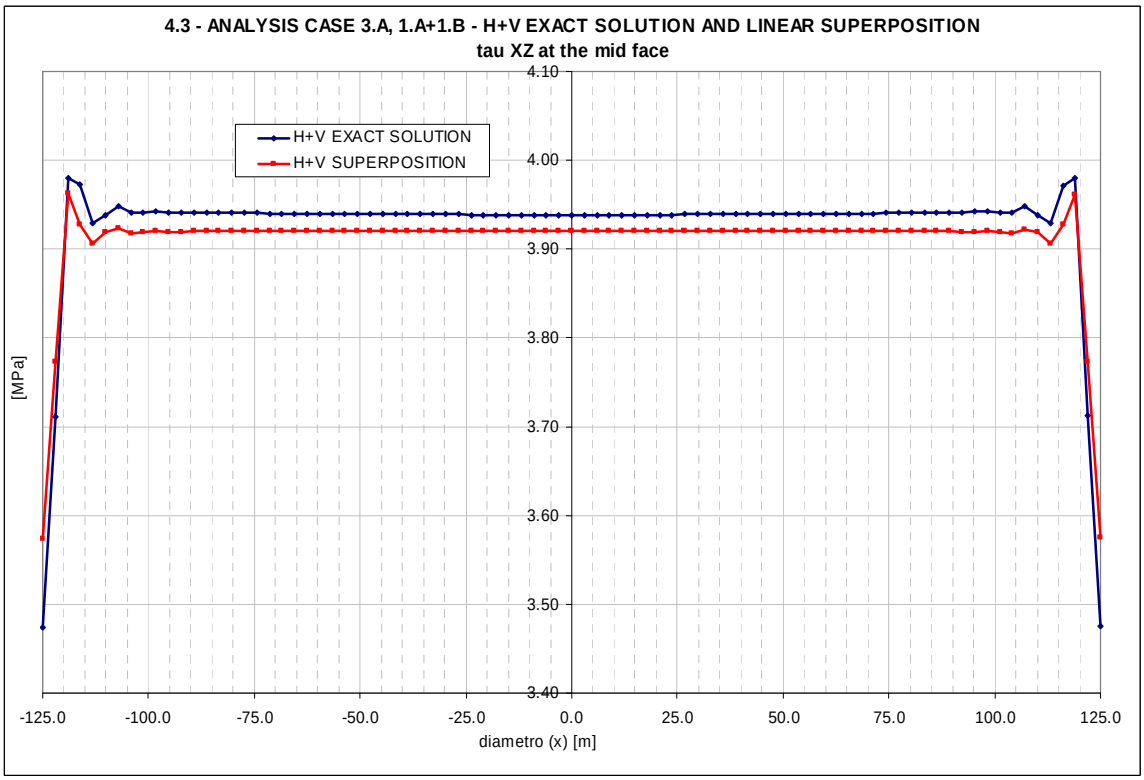
4.3 - ANALYSIS CASE 3.A, 1.A+1.B - H+V EXACT SOLUTION AND LINEAR SUPERPOSITION
tau XZ at the mid face
H+V EXACT SOLUTION
H+V SUPERPOSITION
[MPa]
4.10
4.00
3.90
3.80
3.70
3.60
3.50
3.40
-125.0
-100.0
-75.0
-50.0
-25.0
0.0
25.0
50.0
75.0
100.0
125.0
diametro (x) [m]

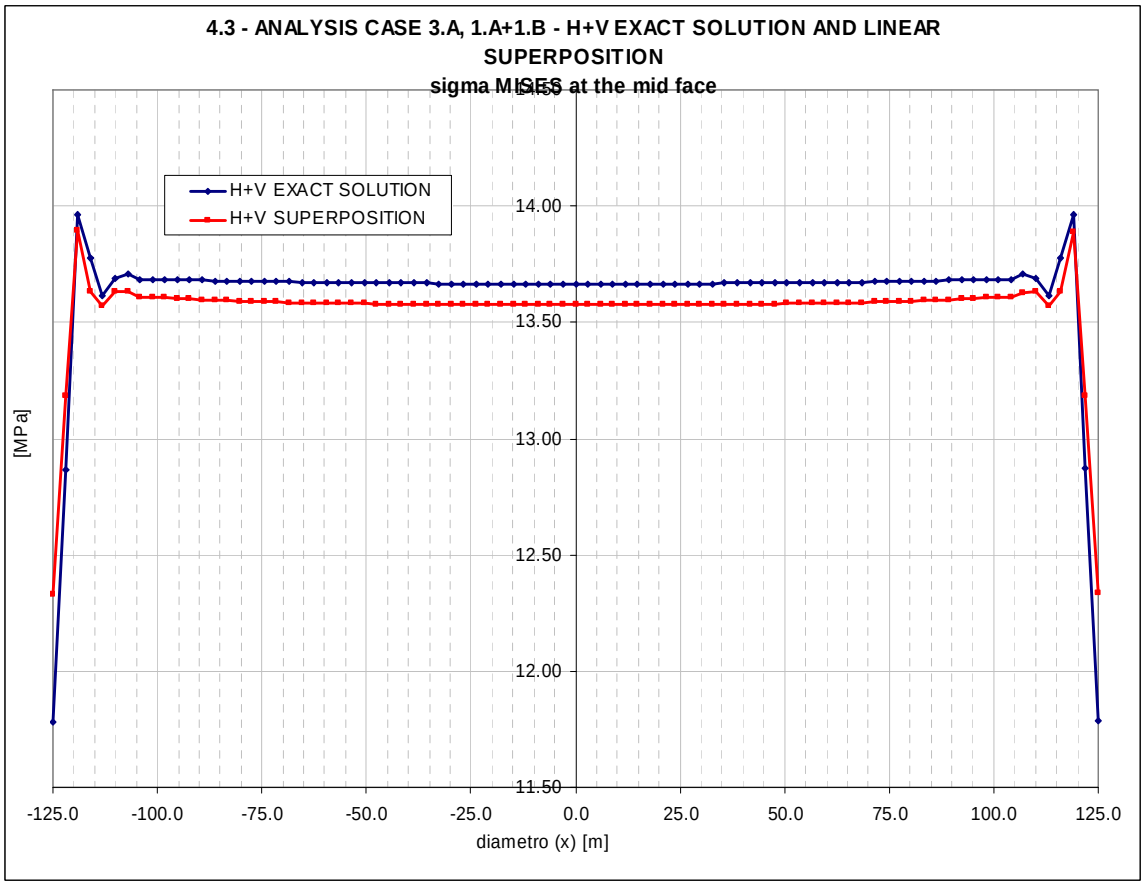
4.3 - ANALYSIS CASE 3.A, 1.A+1.B - H+V EXACT SOLUTION AND LINEAR SUPERPOSITION
sigma MISES at the mid face
H+V EXACT SOLUTION
H+V SUPERPOSITION
[MPa]
14.00
13.50
13.00
12.50
12.00
11.50
-125.0
-100.0
-75.0
-50.0
-25.0
0.0
25.0
50.0
75.0
100.0
125.0
diametro (x) [m]